

Interplanetary magnetic field rotations followed from L1 to the ground: the response of the Earth's magnetosphere as seen by multi-spacecraft and ground-based observations

M. Volwerk¹, J. Berchem², Y. V. Bogdanova³, O. D. Constantinescu⁴, M. W. Dunlop⁵, J. P. Eastwood⁶, P. Escoubet⁷, A. N. Fazakerley³, H. Frey⁸, H. Hasegawa⁹, B. Lavraud^{10,11}, E. V. Panov¹, C. Shen¹², J. K. Shi¹², M. G. G. T. Taylor⁷, J. Wang¹³, J. A. Wild¹⁴, Q. H. Zhang¹⁵, O. Amm¹⁶, and J. M. Weygand²

¹Space Research Institute, Austrian Academy of Sciences, 8042 Graz, Austria

²IGPP UCLA, Los Angeles, CA, USA

³Mullard Space Science Laboratory, University College London, Dorking, UK

⁴Institut für Geophysik und extraterrestrische Physik, Technische Universität, 38106 Braunschweig, Germany

⁵Department of Space Sciences, Rutherford Appleton Laboratory, Didcot, UK

⁶Blackett Laboratory, Imperial College London, London, UK

⁷ESTEC, Noordwijk, The Netherlands

⁸SSL, University of California, Berkeley, CA, USA

⁹Institute of Space and Astronautical Science, JAXA, Sagami-hara, Japan

¹⁰Centre d'Étude Spatiale des Rayonnements, Université de Toulouse, Toulouse, France

¹¹Centre National de la Recherche Scientifique, UMR 5187, Toulouse, France

¹²CSSAR, Chinese Academy of Sciences, Beijing, China

¹³Peking University, Beijing, China

¹⁴Department of Physics, Lancaster University, Lancaster, UK

¹⁵SOA Key Laboratory for Polar Science, Polar Research Institute of China, Shanghai, China

¹⁶Arctic Research Unit, Finnish Meteorological Institute, Helsinki, Finland

Received: 2 November 2010 – Revised: 15 July 2011 – Accepted: 30 August 2011 – Published: 8 September 2011

Abstract. A study of the interaction of solar wind magnetic field rotations with the Earth's magnetosphere is performed. For this event there is, for the first time, a full coverage over the dayside magnetosphere with multiple (multi)spacecraft missions from dawn to dusk, combined with ground magnetometers, radar and an auroral camera, this gives a unique coverage of the response of the Earth's magnetosphere. After a long period of southward IMF B_z and high dynamic pressure of the solar wind, the Earth's magnetosphere is eroded and compressed and reacts quickly to the turning of the magnetic field. We use data from the solar wind monitors ACE and Wind and from magnetospheric missions Cluster, THEMIS, DoubleStar and Geotail to investigate the behaviour of the magnetic rotations as they move through the bow shock and magnetosheath. The response of the magne-

tosphere is investigated through ground magnetometers and auroral keograms. It is found that the solar wind magnetic field drapes over the magnetopause, while still co-moving with the plasma flow at the flanks. The magnetopause reacts quickly to IMF B_z changes, setting up field aligned currents, poleward moving aurorae and strong ionospheric convection. Timing of the structures between the solar wind, magnetosheath and the ground shows that the advection time of the structures, using the solar wind velocity, correlates well with the timing differences between the spacecraft. The reaction time of the magnetopause and the ionospheric current systems to changes in the magnetosheath B_z seem to be almost immediate, allowing for the advection of the structure measured by the spacecraft closest to the magnetopause.

Keywords. Magnetospheric physics (Magnetosheath; Magnetosphere-ionosphere interactions; Solar wind-magnetosphere interactions)



Correspondence to: M. Volwerk
(martin.volwerk@oeaw.ac.at)

1 Introduction

The main driver of the dynamics of Earth's magnetosphere is the solar wind, through e.g. reconnection at the magnetopause during southward Interplanetary Magnetic Field (IMF) B_z eroding the magnetic field at the dayside or compression of the magnetosphere during high ram pressure with northward IMF B_z . Nishida (1983) already described how the IMF influences the Earth's magnetosphere. The interaction of specific structures in the solar wind and how they transport energy from the solar wind to the magnetosphere is discussed e.g. by Lundin (1988). The compression of the magnetosphere by a period of high ram pressure solar wind, ~ 4.5 nPa (similar to the ram pressure for the event discussed in this current paper) was observed during a passage of WIND through the magnetosheath and magnetopause (Phan et al., 1996). The reaction of the Earth's magnetosphere to interplanetary coronal mass ejections (ICMEs), observed by ACE and Wind, was studied in a set of papers by e.g. Farrugia et al. (1993a,b, 1995, 2002) and for low Mach number CMEs by e.g. Lavraud and Borovsky (2008).

Single spacecraft measurements of the solar wind interaction with the bow shock and the magnetopause include studies of Flux Transfer Events (FTEs) by Geotail (see e.g. Sibeck and Siscoe, 1984; Korotova et al., 2009). The motion of the magnetopause and its statistical location was studied using Geotail (Ivchenko et al., 2000). And the erosion of the magnetopause during southward IMF was studied by e.g. Pudovkin et al. (1997); Shue et al. (2001).

In this age of multi-spacecraft missions, as Cluster and THEMIS, it has become easier to investigate the motion of solar wind structures and their properties in various locations. For instance FTEs have been studied with THEMIS by Wild et al. (2005); Fear et al. (2008); Lui et al. (2008); Hasegawa et al. (2010) and with Cluster by Lockwood et al. (2001); Wang et al. (2007). The motion of interplanetary shocks through the magnetosheath have been studied using Cluster (Keika et al., 2008, 2009; Pallochia et al., 2010) and THEMIS (Zhang et al., 2009).

The connection between something happening in the solar wind, such as an IMF rotation, and what happens deeper in the magnetosphere has been studied by Sandholt et al. (1998, 2004, and references therein). They discuss the dayside aurora and its relation to the IMF magnetic field orientation. They show that for "intermediate" clock angle (B_y dominant and $90^\circ < \theta < 135^\circ$) the aurora moves to higher latitudes. For strongly southward field ($135^\circ < \theta < 180^\circ$) they find a strong erosion of the magnetopause. Sandholt and Farrugia (2002) found that observations of the dynamics of the aurora could well be used to monitor global changes in the magnetospheric magnetic topology.

The changes in the location of the aurora are often related to changes in the location of the open-closed magnetic field line boundary. The determination of the location of the open-closed boundary can be done by various methods. In the

case of the dawn sector Wild et al. (2004) used SuperDARN, IMAGE, Cluster, Fast and DMSP data to find this location. It was found that narrow band UV emissions (130–140 nm) were most reliable.

The motion of the magnetopause (and the bow shock) caused by its interaction with an interplanetary shock was studied by Zhang et al. (2009), where they found that the magnetopause moves Earthward at a velocity of ~ 47 km s⁻¹. This Earthward motion is caused by the increase of dynamic pressure and not through erosion of the magnetopause. Indeed, the response of the magnetosphere to changes in dynamic pressure in the solar wind have been discussed by Sibeck (1990); Sibeck and Gosling (1996). The response to variations in the IMF direction were discussed in Sibeck et al. (2000), where it was found that the magnetopause moved outward when the magnitude of the IMF B_y decreased. However, the link between IMF B_z and region 1 Birkeland currents, together with the inward motion of the magnetopause and a decrease in magnetospheric field strength was shown in Sibeck et al. (1991).

The erosion of the magnetopause through southward IMF B_z is discussed by e.g. Mühlbachler et al. (2003, 2004) where the reduction of the total magnetic field at geostationary orbit is modeled as a function of the IMF B_z . Lockwood et al. (2005) also showed the erosion for southward IMF, however, they found that the open-closed boundary moves poleward regardless of IMF direction when there is a substorm growth phase in the tail.

Lately, some studies have been done on the open-closed field line boundary and the cusp and the dependence on the IMF (Pitout et al., 2006; Hu et al., 2007; Cai et al., 2009), where it was found that the reconnection line moves equatorward/poleward of the cusp when the IMF changes sign, and compatible with the pictures obtained from statistical studies (Lavraud et al., 2004, 2005). The cusp was observed to react rather fast to local (i.e. lagged to the position of Cluster) turnings of the IMF as also shown in numerical modeling by Wiltberger et al. (2003).

In the past the lack of simultaneous coverage by spacecraft in the solar wind and in the magnetosphere has prevented (comprehensive) coordinated studies of the interaction of IMF rotations with the magnetosphere. In this paper we combine the data from a special conjunction of THEMIS and Cluster, with the former near the dusk flank and the latter near the dawn flank. With the help of two other missions, DoubleStar and Geotail, we can get information about what is happening near the nose of the magnetopause. The solar wind monitors ACE and Wind show what kind of structures interact with the bow shock and magnetopause. Ground based magnetometers, ionospheric radars and an auroral camera show what is happening inside the magnetosphere. This is the first time that such a comprehensive data set is put together to investigate the response of the Earth's magnetosphere to rotations in the solar wind magnetic field.

In this paper we investigate how north-south rotations of the IMF, as measured by Wind and ACE are interacting with the Earth's magnetosphere and what signatures are measured on the ground. We use data from various space experiments: in the solar wind ACE and Wind; in the magnetosheath THEMIS, Cluster, DoubleStar and Geotail; on the ground CARISMA, south pole auroral camera, SuperDARN and IMAGE and equivalent currents are determined from data delivered by 48 stations from various ground magnetometer chains (CANMOS, CARISMA, GIMA, Greenland, MACCS and THEMIS GMAG). The paper is built up in the following way: Sect. 2.1 discusses the observations by ACE and Wind and the IMF rotations are identified and the properties of the rotational fronts passing by the spacecraft is studied. Section 2.2 discusses the observations of these rotations by the spacecraft in the Earth's magnetosheath. Section 2.3 looks at the behaviour of the magnetopause and the aurora and Sect. 2.4 discusses the data from ground magnetometers and the SuperDARN radars. In Sect. 3 we discuss the data presented in the previous section and in Sect. 4 a summary and conclusion is given.

2 The data

Unless stated otherwise, the data from the spacecraft are given in the GSE coordinate system.

2.1 Observations in the solar Wind

On 14 June 2007, Wind, located at $(262, 33, 24) R_E$, and ACE, located at $(232, -37, 14) R_E$, measured the solar wind magnetic field (Smith et al., 1998; Lepping et al., 1995) and plasma (McComas et al., 1998; Lin et al., 1995) shown in Fig. 1. During the interval of 14:00–20:00 UT it is clear in the data that there are several magnetic structures in the solar wind, mostly rotations of the field. We have marked the north-south (NS) and south-north (SN) IMF rotations with yellow shadings in Fig. 1 and numbered them 1 through 6. There are changes in magnetic field magnitude, B_t , up to 30% for some field rotations, at the first SN rotation # 1 at $\sim 16:18$ UT the total field increases by 2 nT and after the first NS crossing (# 2) the field decreases by 2 nT. After $\sim 18:38$ UT there is a significant change in B_t during the NS rotation # 6 with a drop of 3 nT.

ACE is lagging Wind by approximately 12 min, which is about twice the solar wind travel time in the x-direction with the solar wind velocity as shown in Fig. 1. This means that these fronts are not moving outward as a plane wave structure with its normal in the x-direction. We will discuss this further below.

The solar wind is rather fast at $\sim 584 \text{ km s}^{-1}$, with a density of $\sim 6 \text{ cm}^{-3}$, which corresponds to a strong dynamic pressure of $P_{\text{dyn}} \approx 4.6 \text{ nPa}$. This leads to a strong compression of the magnetosphere. Furthermore, the solar wind mag-

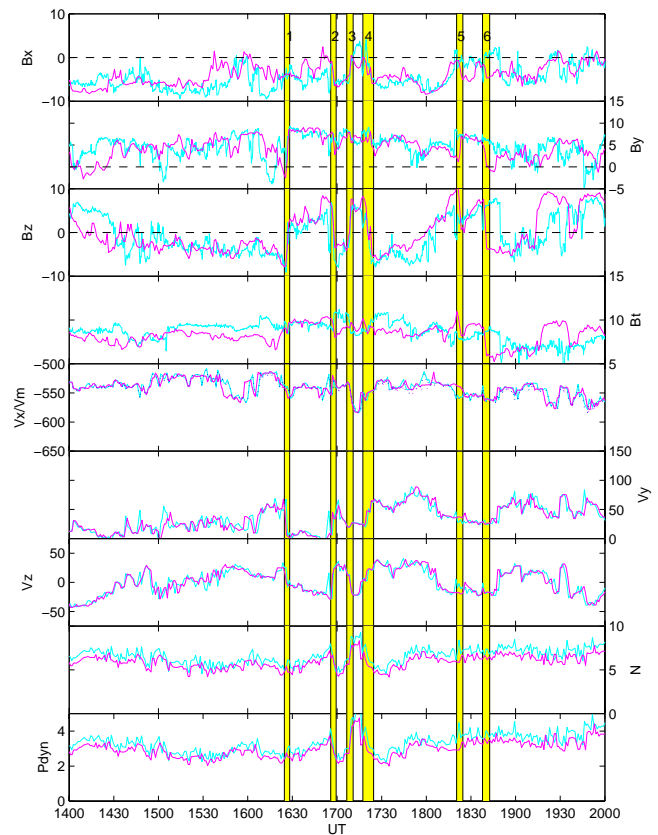


Fig. 1. Wind (magenta) and ACE (blue) data for 14 June 2007, showing in GSE coordinates the solar wind magnetic field parameters (3 components and total field) and the solar wind velocity (3 components) and density. The data from ACE have been shifted backwards in time by 12 min. The yellow shaded areas are the six magnetic field rotations that will be discussed in this paper.

netic field was southward since $\sim 14:30$ UT (see Fig. 1) and thus a strong erosion of the magnetosphere is expected (this will be discussed in Sect. 2.3 below).

For the purpose of this paper, we identified the following structures in the Wind data during the interval 16:00–19:00 UT (magenta in Fig. 1). First there are two south-north – north-south (SN-NS) turnings of the solar wind magnetic field starting at $\sim 16:26$ UT (# 1) and ending at $\sim 16:58$ UT (# 2) and then starting at $\sim 17:06$ UT (# 3) and ending at $\sim 17:24$ UT (# 4). These structures are followed by a saw-tooth looking behaviour, i.e. a gradual SN rotation of the magnetic field starting at $\sim 17:46$ UT followed by a fast NS rotation at $\sim 18:21$ UT (# 5), followed by another slow SN rotation and again a fast NS rotation at $\sim 18:38$ UT (# 6).

A minimum variance analysis was performed on the magnetic field data for the rotations. The results can be found in Table 1 and the specific intervals are highlighted in Figs. 1 and 2. The normal of rotation # 1 has only slightly different values at Wind and ACE, so we can assume a plane propagating wave. The front is tilted in the XY-plane by $\sim 20^\circ$ with

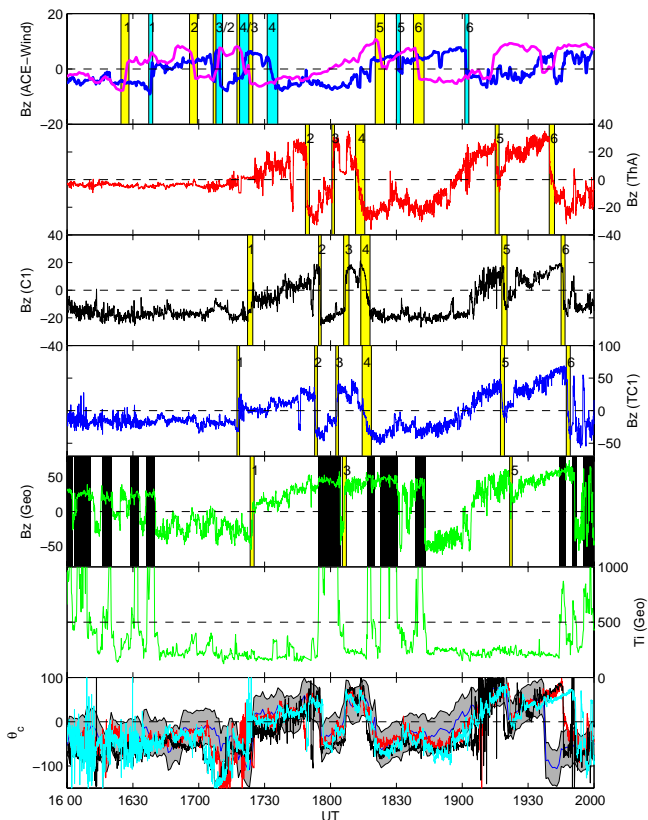


Fig. 2. The B_z data for ACE (blue) and Wind (magenta), THEMIS A, Cluster 1, TC1 and Geotail. The shaded (yellow for ACE and cyan for Wind in the top panel) and numbered areas are the time intervals for which minimum variance analysis was performed (the results shown in Table 1). The black shaded intervals in the Geotail panel show where the spacecraft was inside the magnetosphere. The bottom panel shows the clock angle of the magnetic field for Wind, THEMIS A, Cluster 1 and TC1, with the data shifted as to match with Cluster 1. The grey shaded area around shows a region of $\theta_{c, \text{wind}} \pm 30^\circ$.

respect to the y-axis. This means that at Y_{ACE} the front needs to move an additional $25 R_E$ to reach the spacecraft, almost doubling the ΔX between Wind and ACE from 30 to $55 R_E$, leading to a ~ 12 min travel time.

Using the criteria by Smith (1973) we have determined whether these rotations of the magnetic field direction are rotational or tangential discontinuities. We have calculated $B_n/B_{1, \text{max}}$ and $\Delta B_{\text{tot}}/B_{1, \text{max}}$, where B_n and B_1 are the magnetic field components in the minimum and maximum variance directions, respectively. According to the qualification by Smith (1973) rotational discontinuities have $B_n/B_{1, \text{max}} > 0.4$ and $\Delta B_{\text{tot}}/B_{1, \text{max}} < 0.22$, whereas tangential discontinuities have $B_n/B_{1, \text{max}} < 0.22$ and $\Delta B_{\text{tot}}/B_{1, \text{max}} > 0.22$. Discontinuities with $B_n/B_{1, \text{max}} < 0.4$ and $\Delta B_{\text{tot}}/B_{1, \text{max}} < 0.22$ are considered ambiguous, and any values outside these three limits are labeled as not fitting any classification.

The results are given in Table 1, which shows that for Wind # 1 is a tangential discontinuity, # 2 is ambiguous and # 3 trough 6 are do not fit in Smith's classification. For ACE we only find that # 5 is a rotational discontinuity and all others do not fit any classification.

It should be noted that for ACE the eigenvalue ratio λ_1/λ_2 of rotations # 2 and 3 is rather large, so the normal direction may not be well defined. In order to be able to make some analysis of the front motion, we have set a, relatively large, limit to the eigenvalue ratio of 0.2. Also, "nested MVA" analysis (see e.g. Zhang et al., 2005; Volwerk, 2006) should give the approximately same normal direction. This analysis showed that there is little difference in the normal determination for slightly different time intervals over the rotations, and did not result in a better ratio for λ_1/λ_2 . For a discussion of the MVA technique and its limitations see e.g. Volwerk (2006) and references therein.

In Fig. 3 left column, we have plotted the normal directions for the first four rotations (# 1 through 4) and the plane of the front for ACE and Wind. These four rotations make up a set of "square wave" fast SN-NS turnings, which we can easily compare with each other. Using the front normals (minimum variance direction) we make an assumption on the shape of the front moving with the solar wind, which is displayed as a yellow curve in the figure.

It is clear that for rotation # 3 the minimum variance direction is very different between ACE and Wind, and it seems that this front is concave as seen from the Earth, instead of plane or convex as one would expect coming from the Sun and as the other three fronts are, see Fig. 3 left column. Such conclusions must be looked at skeptically, though, because of the ambiguous normal direction.

Not only is there a difference in the "front normal" of the magnetic field rotations # 2, 3 and 4 for ACE and Wind, the shapes of the structures are also different, as can be seen in Fig. 1. At this point, it is difficult to say whether these changes in shape are temporal variation related to the travel time from ACE to Wind or if they are spatial changes related to the different locations of the two spacecraft in the solar wind. As for rotations # 2 and 3 the MVA direction is well determined for Wind, we can make a similar calculation as for rotation # 1 to check whether the front is a plane or a convex/concave structure. Assuming a plane propagating front we find for rotations # 2 and 3 an angle/extra ΔX of $32^\circ/44 R_E$ and $47^\circ/75 R_E$, respectively. With a nearly constant solar wind velocity, this means that the time delay between Wind and ACE should be greater than the ~ 12 min as determined for # 1. Observed is that the delay has not changed, indicating that the front has to be concave, as seen from the Earth. Rotation # 4 shows a different sign y-component of the normal which results in an angle/extra ΔX of $-17^\circ/21 R_E$. Again, assuming constant solar wind velocity and constant time delay between Wind and ACE, the front needs to be convex. This is consistent with the (badly) determined normals for ACE.

Table 1. Minimum variance directions for the south-north and north-south turnings for the various spacecraft for the intervals marked in Fig. 2, including the ratio of minimum and intermediate eigenvalue and discontinuity parameters. Any values in italics mean that the minimum variance direction was not well defined.

Time	λ_1/λ_2	Wind	λ_1/λ_2	ACE
1	$<10^{-3}$	(0.88, 0.32, -0.34)	0.07	(0.87, 0.45, -0.15)
2	$<10^{-3}$	(0.65, 0.41, -0.63)	0.4	(0.94, -0.10, -0.33)
3	0.02	(0.67, 0.72, -0.15)	0.4	(0.31, -0.79, 0.53)
4	0.06	(0.89, -0.25, -0.36)	0.15	(0.72, 0.38, -0.58)
5	0.40	(0.88, 0.45, -0.11)	0.11	(0.78, 0.11, -0.61)
6	0.12	(0.85, 0.35, -0.39)	0.21	(0.87, -0.21, -0.44)

Time	$B_n/B_{1,max}$	$\Delta B_{tot}/B_{1,max}$	$B_n/B_{1,max}$	$\Delta B_{tot}/B_{1,max}$
1	0.19	0.28	0.26	1.43
2	0.11	0.03	0.67	0.88
3	0.56	0.91	0.88	0.01
4	0.55	0.56	0.41	0.60
5	0.12	1.17	0.41	1.19
6	0.30	0.43	0.52	0.14

	λ_1/λ_2	C1	λ_1/λ_2	ThA
1	0.3	(0.61, -0.75, -0.21)	-	-
2	0.6	(0.92, 0.19, -0.34)	0.2	(0.67, 0.73, -0.08)
3	0.2	(0.13, 0.96, 0.24)	0.2	(0.90, 0.42, -0.05)
4	0.1	(0.57, -0.61, 0.54)	0.3	(0.94, 0.30, -0.13)
5	0.7	(0.80, -0.53, -0.25)	0.19	(0.93, 0.34, 0.09)
6	0.22	(0.36, -0.85, 0.39)	0.25	(0.80, 0.59, -0.03)

	Timing	C	Timing	Th
1	tim	(0.94, -0.17, -0.28)	tim	(0.98, -0.15, 0.13)
2	tim	(0.97, -0.11, -0.23)	tim	-
3	tim	(0.99, 0.01, -0.15)	tim	(0.97, -0.18, 0.12)
4	tim	(0.76, 0.56, -0.32)	tim	(0.98, -0.16, 0.13)
5	tim	(0.94, 0.33, -0.08)	tim	(0.90, -0.26, 0.34)
6	tim	(0.97, -0.09, 0.23)	tim	(0.99, -0.07, 0.14)

	λ_1/λ_2	TC1	λ_1/λ_2	Geo
1	0.6	(0.67, -0.67, 0.29)	0.16	(0.86, -0.50, -0.10)
2	0.2	(0.90, 0.07, -0.42)	-	-
3	0.09	(0.89, -0.16, 0.42)	0.14	(0.86, -0.50, -0.01)
4	0.09	(0.94, -0.12, 0.31)	-	-

The sawtooth-looking rotation #5 has slightly different front normals for ACE and Wind, however, the main difference between the two spacecraft is the time length difference and normal direction for the second sawtooth-looking rotation # 6. Figure 1 shows that rotation # 6 happens approximately 12 min later for ACE as compared with Wind in the time shifted data set. It will be shown below that all magnetosheath spacecraft observe the longer sawtooth-looking structure as observed by ACE. The normals for # 5 at Wind and # 6 at ACE are badly determined, however similar to above a case can be made that the normals are acceptable for rotation # 5 and the propagation of the rotational front. However, for rotation # 6 it is not so clear. In the XY-plane

the two normals are pointed towards each other (i.e. opposite sign of y-component) and thus a concave structure for the front can be assumed comparable with that of rotation # 3. From the inferred shape of the front there is no compelling reason for the second interval (between # 5 and # 6) to be so much shorter, thus a spatial difference in the solar wind structure must be assumed to explain this phenomenon.

2.2 Observations in the Earth’s magnetosheath

During the time interval discussed in the previous subsection, several spacecraft are located in the magnetosheath: THEMIS at ~15:00 LT, Cluster at ~05:00 LT, DoubleStar TC1 is near local noon and Geotail skims along the

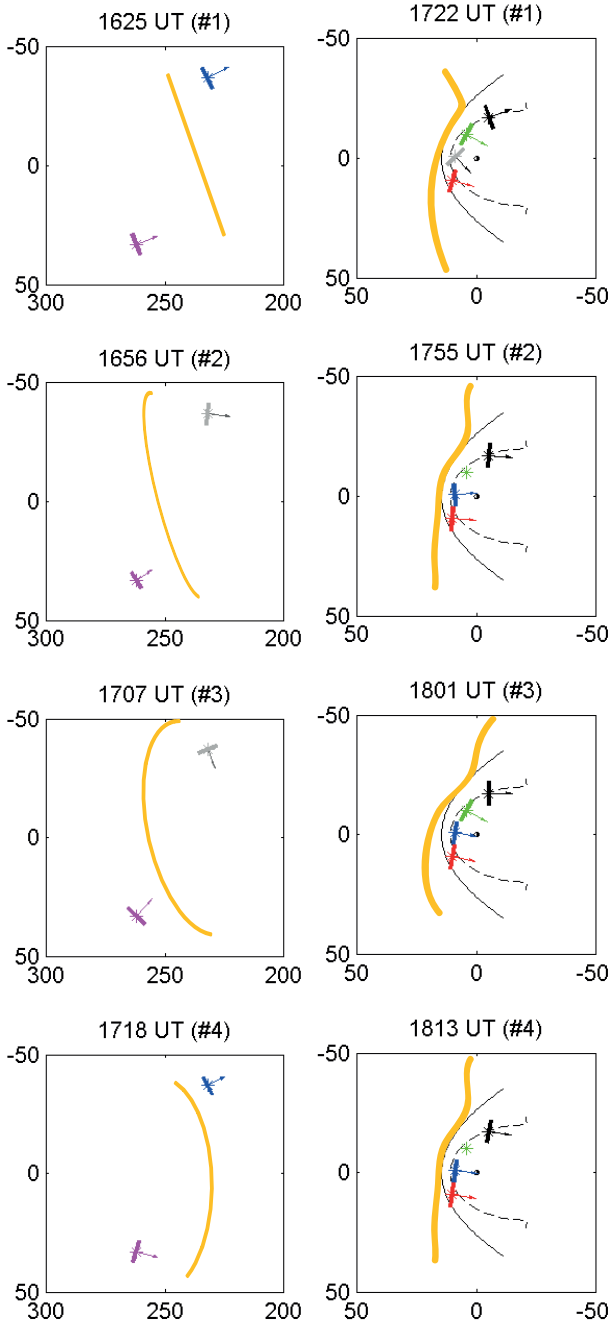


Fig. 3. Left column: the location of ACE (blue) and Wind (magenta) and the minimum variance direction of the magnetic field rotations as arrows and the tangential plane in the XY-plane. The yellow curve shows an interpretation of the spatial shape of the fronts moving with the solar wind and should only be used as a guide. Right column: the location of Cluster (black), Geotail (green) DoubleStar TC1 (blue) and THEMIS (red) in the XY-plane, with the average location of the bow shock (solid black) and magnetopause (dashed black) taken from Fairfield (1971) and the yellow curve shows how the draping of the solar wind over the magnetopause can look like. Spacecraft labeled in grey indicate an ill-defined normal direction.

magnetopause from ~07:00 to ~11:30 LT. The locations of the spacecraft are shown in Fig. 4.

We use data from the flux gate magnetometers on the various spacecraft (Auster et al., 2008; Balogh et al., 2001; Carr et al., 2005; Kokubun et al., 1994). The B_z of all spacecraft are shown in Fig. 2. It is clear that THEMIS, Cluster and TC1 show a similar B_z -behaviour as the solar wind monitors. The first clear difference between the solar wind and the magnetosheath is that the amplitude of the magnetic rotations is much larger in the magnetosheath. Naturally, such an amplification is expected after a crossing of the Earth’s bow shock (see e.g. Sckopke et al., 1983; Burgess, 1995).

The THEMIS spacecraft are close to the bow shock after having crossed it and entered the magnetosheath at ~17:25 UT. THEMIS A even crosses back into the solar wind at ~18:06 UT, in the middle of the SN-NS rotation while B_z was northward. Therefore, we use THEMIS to check the shock relation for a quasi-perpendicular bow shock. For the exactly perpendicular shock one can write the following relation between upstream (u) and downstream (d) shock normal velocity and shock tangential magnetic field (see e.g. Burgess, 1995):

$$v_{un} \mathbf{B}_{ut} = v_{dn} \mathbf{B}_{dt}. \tag{1}$$

In order to find the normal of the bow shock we use coplanarity theorem (Schwartz, 1998). Using the various techniques we find an average normal of $\hat{n} \approx (0.87, 0.42, -0.25)$. Similarly, in order to find the speed of the bow shock in the spacecraft frame of reference we use the mass-flux algorithm (Schwartz, 1998), which leads to $v_{sh} \approx 38.5 \text{ km s}^{-1}$ along the normal. Having determined these two quantities for the bow shock we can then relate the upstream and downstream quantities through Eq. (1). For example comparing the minimum in B_z at ThA near ~18:00 UT compared to the same minimum in the solar wind data: upstream $v_n B_t \approx 4.72 \text{ mV m}^{-1}$ and downstream 4.86 mV m^{-1} , a rather good agreement.

A minimum variance analysis was performed on the same structures as in the ACE and Wind data, for the magnetosheath spacecraft. The result is shown in Table 1 and the intervals are highlighted in Fig. 2. The MVA determination has a very large eigen value ratio λ_1/λ_2 for many of the structures. Therefore, the normals for the multi-spacecraft missions Cluster and THEMIS have also been determined using timing analysis. We have performed timing analysis (Harvey, 1998) on the magnetic field data for all 6 structures, using the $B_x = 0$ crossing for all spacecraft. In Fig. 3 right column the structure normals and their tangents are plotted, where the locations of the bow shock (solid line) and magnetopause (dashed line) are taken from Fairfield (1971). The figure shows how the magnetic field (structures) get draped over the Earth’s magnetopause at the nose of the magnetopause and pulled out again at the flanks. The bottom panel in Fig. 2 shows the clock angle of the magnetic field, defined as $\theta = \text{atan}\{B_z/B_y\}$, where the grey shaded area around the

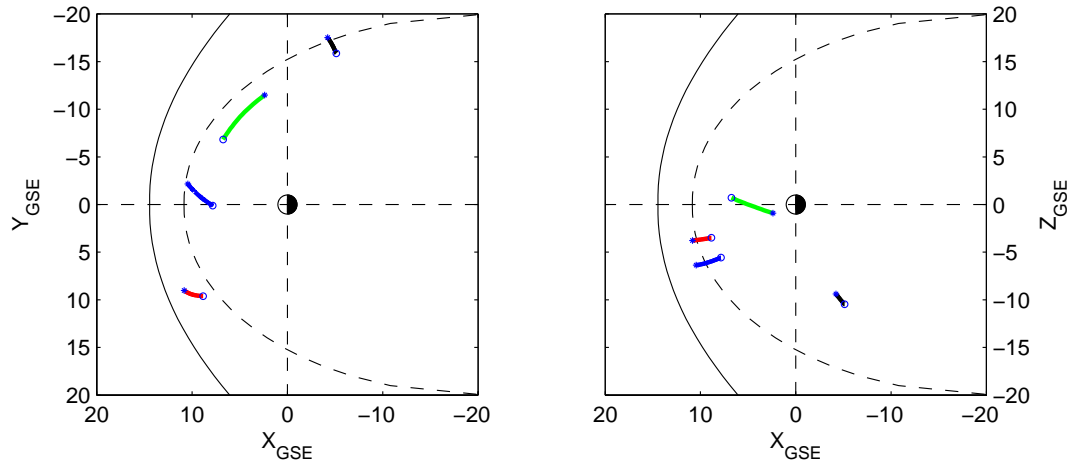


Fig. 4. Schematic of the location of the near-Earth spacecraft in the XY- and XZ-plane over the period of 16:00 (*) till 20:00 (O) UT, which shows how the spacecraft are moving in the magnetosheath (C1 black, Geotail green, TC1 blue, ThA red). The solid curved line is the bow shock and the dashed curved line is the magnetopause as in Fig. 3.

Wind trace shows $\theta_W \pm 30^\circ$ as Coleman (2005) showed that 70 % of the draping events fall within this region.

Similarly, we can compare the velocities of the magnetic field structures upstream and downstream of the shock using spacecraft for which plasma measurements are available, i.e. Cluster (Rème et al., 2001) and THEMIS (McFadden et al., 2008). The temporal length of the second SN-NS structure is slightly different for both solar wind monitors: ACE shows a time interval of ~ 12.3 min, whereas Wind shows a time interval of ~ 14.0 min. For the spacecraft in the magnetosheath we find that the time interval for Cluster is ~ 9.6 min, for THEMIS ~ 11.7 min and for TC1 ~ 12.1 min. Assuming continuity and frozen-in field, the ratio of the time intervals R_T in solar wind and magnetosheath should be comparable to the ratio of the plasma velocity R_v in the solar wind and in the magnetosheath. We find the following ratios:

1. Cluster:
 - (a) ACE $R_T \approx 0.78 - R_v \approx 0.69$
 - (b) Wind $R_T \approx 0.69 - R_v \approx 0.69$
2. THEMIS:
 - (a) ACE $R_T \approx 0.95 - R_v \approx 0.46$
 - (b) Wind $R_T \approx 0.83 - R_v \approx 0.46$
3. TC1:
 - (a) ACE $R_T \approx 0.98 - R_v$ NA
 - (b) Wind $R_T \approx 0.86 - R_v$ NA

This means there is a good/reasonable correlation between Cluster and Wind/ACE. However, there is very little agreement between THEMIS and either ACE or Wind. Possibly, this could be related to the “squeezing” of the magnetic flux tube as described by Zwan and Wolf (1976) after it has moved into the magnetosheath proper. Near the

quasi-perpendicular shock, the crossing of the bow shock can squeeze the plasma out of the magnetic flux tube along the field lines, whereby the plasma pressure is reduced and the flux tube itself will become thinner because of the non-changing magnetic tension. The assumptions made in the bullet list above are no longer valid then, and thus the calculated ratios will not be in agreement.

In Table 3 the result of the timing analysis is shown for rotations # 3, 4, 5, and 6. These rotations were chosen as they represent two different kind of structures in the solar wind, the “square” and the “sawtooth-looking” rotations. Rotation # 1 is rather unclear in the THEMIS data and thus this one and # 2 have been omitted here. The determined structure velocity is compared with the measured plasma velocity. As the timing method only determines the velocity of the structure along the normal (and thus implicitly also the normal itself), we have also projected the plasma velocity onto the normal direction. In Fig. 5 we show a graphical representation of the result. The velocity for rotation # 4 at Cluster is ill defined because of a variation in the C2 magnetic profile, which also means that the normal is ill defined. However, for the Cluster spacecraft it seems clear that the motion of the magnetic structure agrees well with the motion of the plasma, i.e. the magnetic field is most likely frozen into the plasma, i.e. the timing analysis will underestimate the actual velocity of the structure (see e.g. Harvey, 1998). For THEMIS the discrepancy between the velocity determined from the timing analysis and that from the plasma instrument is greater. The constellation of the THEMIS spacecraft, however, is not good for timing analysis. When the spacecraft are in a quasi-2-D or quasi-1-D configuration, the correct determination of the normal and velocity loses integrity as the “disappearing” dimensions cannot be probed and thus do not add their contribution to the determination of the normal. For an overview

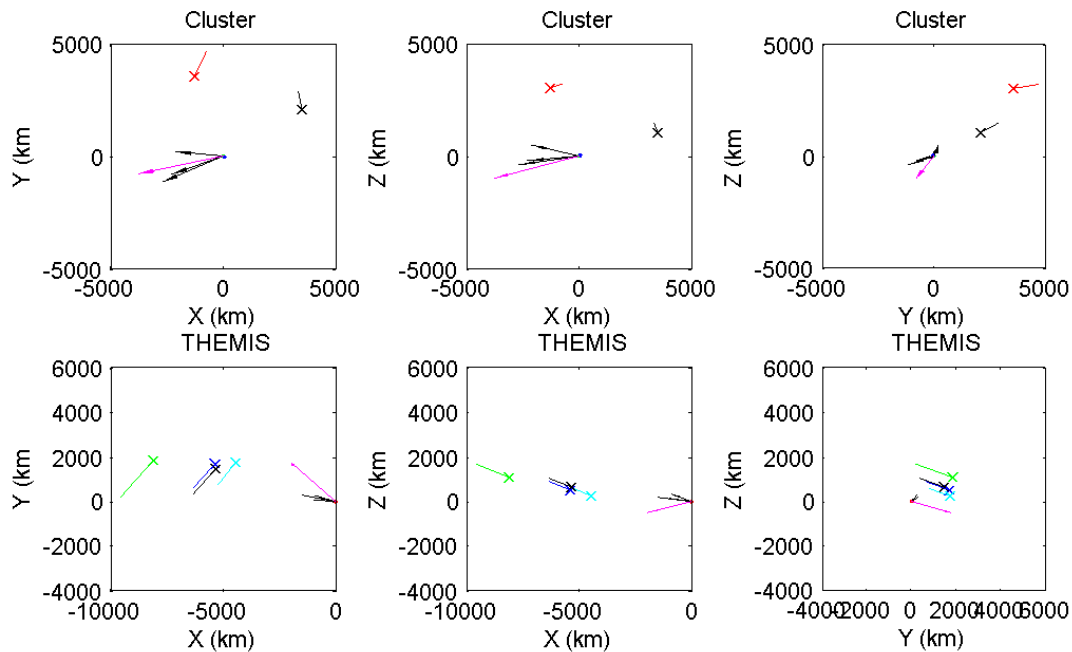


Fig. 5. The location (marked by x) and motion (marked by a line starting from the x) of the cluster (top) and THEMIS (bottom) spacecraft during the period 17:00–19:00 UT. The plasma flow velocity is shown as a pink arrow from C1 and ThA. The structure velocities, determined by timing analysis, are shown as black arrows.

of multi-satellite techniques see e.g. Paschmann and Daly (1998); Volwerk (2006); Paschmann and Daly (2008). We will return to this in the discussion section.

The magnetic field structures observed by the solar wind monitors were slightly different in shape, where it was not known if it were temporal or spatial differences that were observed. Comparison of the sawtooth-looking structure with the solar wind monitors shows that in shape there is good agreement between Wind, THEMIS and TC1 (slow ramp up of B_z), then there is the other combination of ACE, Cluster and Geotail (quick jump of B_z). These combinations are also related to the spacecraft positions, based on the spacecraft being located on the dusk or dawn side of the Earth, with TC1 near noon counted as a dusk. This clearly indicates that there is a dawn-dusk spatial variation of the structure in the solar wind.

In Table 2 we show the time difference between the structures observed by Wind (farthest from the Earth) and the other spacecraft and in the magnetosheath the time difference between ThA (closest to the bow shock) and the other near-Earth missions. We have chosen structure # 3 (see Fig. 2) and the sharp drops in the middle and at the end of the sawtooth-looking structure (# 5 and 6), which are available, and clear sharp structures, in all spacecraft B_z signatures (albeit that for Geotail the latter may be in the magnetosphere). There is good agreement with ΔT_W for # 3 and # 5, but there is a discrepancy of ~ 0.2 h for # 6, i.e. there is a structural difference of 0.2 between the ΔT_W for rotations # 3/5 and rotation # 6. This difference in timing between Wind and the other space-

craft is caused by a variation in the magnetic structure that is only observed by Wind. Clearly, in Fig. 1 panel B_z it can be seen that ACE and Wind do not show the same rotation. The rising part of Wind at $\sim 18:30$ UT is shorter by ~ 12 min when compared with ACE and the spacecraft in the magnetosheath. Table 1 shows that the normals for rotations # 5 and 6 have the same direction (albeit # 5 is badly determined for Wind) thus it seems unlikely that the previously determined curvature of the front is responsible for the difference in duration.

Also note that the time differences between ThA and the other magnetosheath spacecraft is different for these structures. For rotation # 3 the order is ThA – TC1 – Geo – C1 whereas for # 5 C1 moves before Geo (ThA – TC1 – C1 – Geo) and for # 6 also C1 also moves before TC1 (ThA – C1 – TC1 – Geo). This could argue for a differently shaped structure crossing the bow shock. We will address this in the discussion section below.

2.3 Observations along the Earth's magnetopause and aurora

After the long period of southward B_z in the solar wind, the magnetopause is very close to the Earth. TC1 is located near local noon at $(9.41, -0.33, -6.22) R_E$ and Geotail is located near $(4.73, -9.39, -1.20) R_E$ around 18:00 UT. Geotail seems to be skimming the magnetopause, the blacked regions in Fig. 2 B_z (Geo) panel are showing the time intervals that Geotail is in the magnetosphere. The magnetospheric

Table 2. Time differences between different spacecraft of observed magnetic structures. Shown are the times of observation in decimal hours and the differences of all spacecraft with Wind (the furthest out) and the differences between all magnetosheath spacecraft and ThA (nearest the bow shock).

SC	# 3	ΔT_W	ΔT_{ThA}	# 5	ΔT_W	ΔT_{ThA}	# 6	ΔT_W	ΔT_{ThA}
Wind	17.14	–	NA	18.39	–	NA	18.66	–	NA
Ace	17.34	0.20	NA	18.52	0.13	NA	19.03	0.37	NA
ThA	18.02	0.88	–	19.26	0.87	–	19.67	1.01	–
C1	18.11	0.97	0.09	19.32	0.93	0.06	19.77	1.11	0.10
TC1	18.05	0.91	0.03	19.31	0.92	0.05	19.80	1.14	0.13
Geo	18.10	0.96	0.08	19.37	0.98	0.11	19.85	[1.19]	[0.18]

Table 3. Shown are the plasma velocity as measured by the spacecraft and the velocity of the magnetic structures resulting from the timing analysis. The time at which the timing analysis has been performed is given for THEMIS A. Also the angle θ between the plasma flow velocity and the structure normal velocity is given. The velocities in italics are the plasma velocity projected onto the normals of the structure. The plasma velocity did not change significantly over the interval and an average value is used for comparison.

Event	UT	Cluster	$ \mathbf{v} $	θ_{Cl}	THEMIS	$ \mathbf{v} $	θ_{Th}
Plasma		(–380, –80, –100)	401		(–200, 175, –50)	270	
3	18:02	(–270, –117, –40)	297	13°	(–150, 29, 19)	154	35°
		(–355, –153, –52)	390		(–215, 41, 27)	221	
4	18:12	(–92, 27, 33)	101	–	(–116, 19, 16)	119	37°
5	19:15	(–231, –82, –21)	246	12°	(–92, 27, 35)	102	39°
		(–368, –130, –33)	392		(–188, 55, 71)	208	
6	19:40	(–215, 20, 50)	222	32°	(–101, 8, 15)	102	41°
		(–328, 30, 73)	337		(–200, 15, 29)	203	

regions are determined from the plasma instrument (Mukai et al., 1994), setting the limit that the ion temperature is greater than 500 eV (see also the T_i panel in Fig. 2). This puts the magnetopause at the subsolar point at a distance well within $10 R_E$.

It is clear from the Geotail B_z and T_i data in Fig. 2 that whenever Geotail is in the Earth’s magnetosphere, the temperature is high and B_z is positive. However, in the last ~10 min of the interval shown in Fig. 2 the temperature $T_i > 500$ eV (much higher than the magnetosheath value of $T_i \approx 250$ eV), but there is a strong oscillation of the B_z from positive to negative. This is accompanied by strong B_y oscillations with $\Delta B_y \approx 50$ nT in phase with B_z . Most likely, Geotail is in a boundary layer and shows the same B_z oscillations as TC1, but this fall outside the scope of this paper.

In Fig. 6 we have plotted the B_z of TC1 and Geotail (with the black markings showing when Geotail is in the magnetosphere) below the keograms for 4278 and 6300 Å from the Amundsen-Scott base at South Pole (lat. -90°). With Geotail skimming the magnetopause we can use TC1 to evaluate the response of the magnetopause to changes in the magnetic field of the magnetosheath upstream.

Looking at the keogram there are two starts of poleward motion of the aurora at ~17:39 and ~18:18 UT, marked with

a green vertical line in Fig. 6, the end of the poleward motion is marked with pink vertical lines at ~18:12 and ~18:33 UT. The poleward motion of the aurora happens when Geotail and TC1 have been showing positive, i.e. northward B_z for a while. This means that the reconnection at the magnetopause has stopped and the magnetosphere is growing outward again, expanding over Geotail for a while. A schematic is shown in Fig. 7, where after the northward turning of the IMF the magnetopause starts to expand outward and envelops Geotail and after the southward turning of the IMF the magnetopause is eroded again and Geotails enters the magnetosheath.

Analysis of the polar motion of the auroral boundary in geomagnetic coordinates shows that it moves with a velocity of 530 m s^{-1} for the interval 17:45–17:58 UT and 370 m s^{-1} for the interval 18:10–18:27 UT. That corresponds to an outward motion of the magnetic field lines in the dayside equatorial plane of 44 km s^{-1} and 32 km s^{-1} , respectively, which is well within the range of velocities determined by e.g. Berchem and Russell (1982). To determine the velocity of the aurora, in each frame a line was drawn from the center of the frame towards the magnetic pole. The lower border of the aurora was determined along that line and the arc position (and thus speed) was determined assuming an altitude of 110 km for

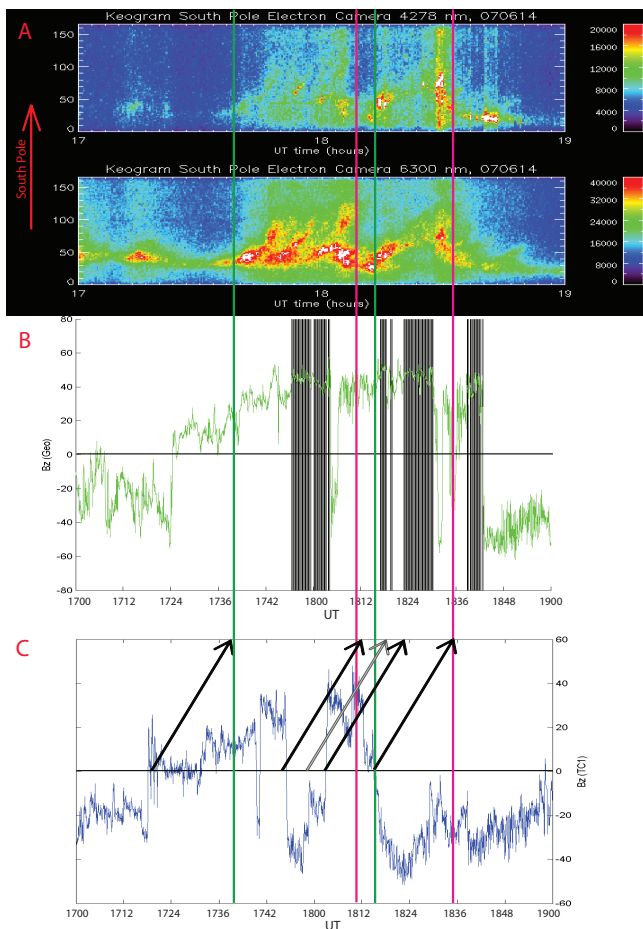


Fig. 6. (A) The south-polar keograms for 4278 and 6300 Å. (B) Geotail B_z , black markings show intervals that the spacecraft is in the magnetosphere. (C) TC1 B_z , with arrows pointing from $B_z = 0$ crossings to change in aurora behaviour. The vertical green and pink lines show the start and end of the poleward motion of the aurora, respectively.

the arc lower border. The estimate for the outward field line motion at the equator is made through a simple dipole magnetic field.

The arrows in the TC1 panel show the relation between the $B_z = 0$ crossings to the changes in the keogram. A remarkable correlation is found for three of the four cases, i.e. a similar time delay of ~ 18 min between TC1 and the keogram signature. When a SN crossing takes place at TC1 this is followed by an expansion of the magnetopause and poleward motion of the aurora, and when a NS crossing takes place, the magnetopause retreats and the poleward motion is stopped. There is a discrepancy with the second onset of poleward motion, unless the grey arrow is used, starting at the near northward crossing at $\sim 17:57$ UT.

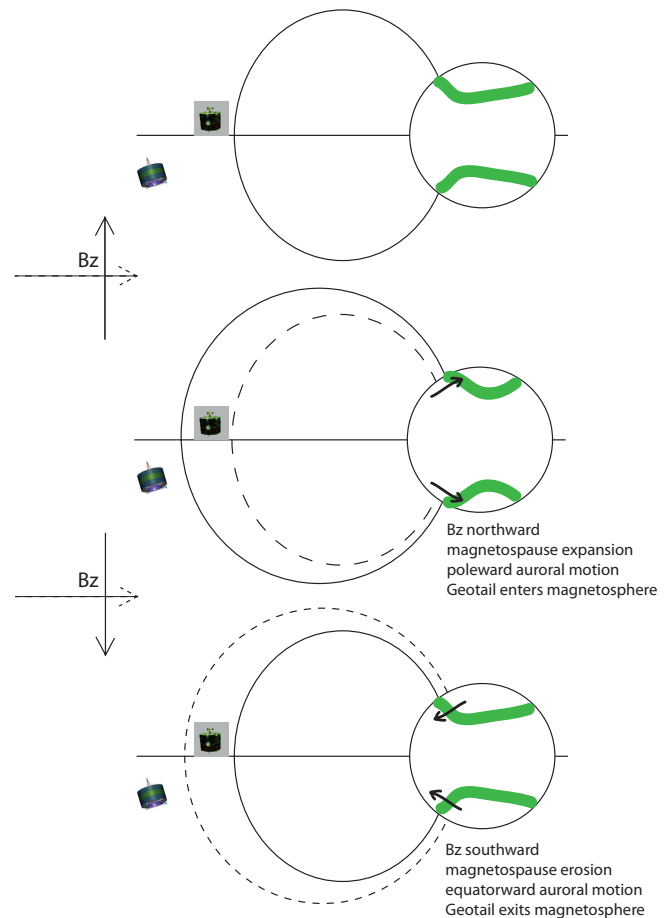


Fig. 7. A schematic showing the behaviour of the magnetopause (solid curved line) and aurora (green slinky) after northward and southward turning of the IMF. Top: the magnetosphere is compressed and both TC1 and Geotail are in the magnetosheath. Middle: after the northward turning the magnetopause expands (from dashed to solid curve) and Geotail moves into the magnetosphere. The aurora moves poleward at the same time. Bottom: after the IMF turns southward, the magnetosphere is eroded again and the magnetopause moves inward again and Geotail exits the magnetosphere. The aurora moves equatorward again.

2.4 Observations on the ground

There are several magnetometer chains that can be used to look at the signatures on the ground. On the day side we use CARISMA around $\sim 10:00$ LT. We show the data for “high” and “low” latitude stations in Fig. 8, where for each station the average value of the magnetic field over the interval is subtracted from the data. The locations of the various ground stations can be found in Table 4.

During the interval of poleward expansion of the aurora discussed above, $\sim 17:39$ – $18:12$ UT, an increase in B_H of up to 400 nT is observed in the high latitude stations. There is not direct evidence of conjugacy of the south polar station and the ground station, however, various studies have

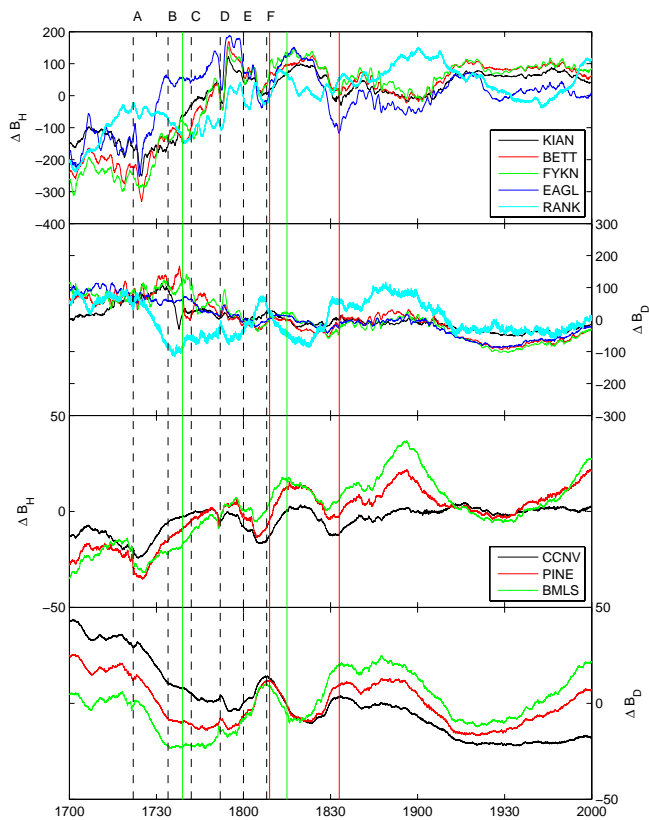


Fig. 8. The ΔB_H and ΔB_D components of the high latitude (top) and low latitude (bottom) ground magnetometers from the Canopus chain. For each trace the mean value over the 3 h period is subtracted. The vertical dashed lines represent the times A through F at which SuperDARN measurements are shown in Fig. 10 and the solid vertical lines show the start and end times of the poleward motion of the aurora as in Fig. 6.

been done where the different hemispheres were compared (see e.g. Østgaard et al., 2004, 2005; Parkinson et al., 2005; Laundal et al., 2010) for symmetries and asymmetries. In this case, the good correlation between the poleward motion of the aurora and the outward motion of the magnetopause as observed by Geotail, leads to the expectation that the ground stations in the Northern Hemisphere show related signatures.

There is a disparity between RANK and the other stations (KIAN, BETT, FYKN, EAGL) in both field components, In B_H RANK increases during a period when the other stations decrease, starting at $\sim 17:12$ UT. At $\sim 17:45$ UT RANK starts to follow the other stations. In B_D RANK decreases when other stations (KIAN, BETT, FYKN) increase and EAGL remains almost constant, starting at $\sim 17:24$ UT. KIAN, BETT and FYKN then start to decrease successively to EAGL level. RANK, however, remains different from the other stations, after $\sim 18:12$ UT, but does follow the trend, only at greater amplitude. This can be caused by both the longitudinal difference between the various stations, with RANK much more east and the latitudinal difference with RANK at the low-

Table 4. Ground based magnetometers geographic location for the THEMIS magnetometers and from the Scandinavian IMAGE chain.

Station	Geo lat	Geo lon	Station	Geo lat	Geo lon
	High latitude			Low latitude	
KIAN	67.0	199.6	CCNV	39.2	240.2
BETT	66.9	208.4	PINE	43.1	257.4
FYKN	66.6	214.8	BMSL	46.2	275.6
EAGL	64.8	218.8			
RANK	62.8	267.9			
NAL	78.9	11.9	BJN	74.5	19.2
LYR	78.2	15.8	SOR	70.5	22.2

est latitude. As will be seen in the equivalent currents plots (Fig. 11), RANK is located below a different current flow system as the other three stations. At $\sim 18:06$ UT EAGL is probably right below the field aligned current, with no B_D variation.

The low latitude stations (CCNV, PINE, BMLS) are located south of RANK. Starting at $\sim 17:24$ UT they show a slowly increasing(decreasing) $B_H(B_D)$ and there is a gradual oscillation of the magnetic field strength indicating a varying ionospheric current.

The sawtooth-looking event does not have any significant signature in the high-latitude stations. The low-latitude stations, including RANK, show a decrease of B_H and B_D starting at $\sim 19:00$ UT, although the lowest latitude station CCNV shows very little variation, suggesting that the erosion has not reached such low latitudes. This is also the time that the sawtooth-looking structure reaches Geotail, the closest spacecraft to the magnetopause. The magnetosheath B_z starts to turn northward again (at $\sim 19:10$ UT), and the erosion of the magnetopause stops. At this point the ground magnetometers have reached a minimum and the B_H and B_D start to increase again, showing the ionospheric and field aligned currents created by the expansion of the magnetopause.

In Fig. 9 the magnetic field data from the IMAGE chain are shown, where again the mean value of each component is subtracted. The IMAGE chain is at the dusk terminator for this time interval. There is strong variation in the magnetic field between 16:30 and 18:00 UT. First there is a strong negative bay in BJA ΔB_x combined with signatures in the other two components. This negative bay moves to higher latitude stations LYR and NAL, approximately 30 min later. However, before this negative bay there is a positive bay in the lowest latitude station SOR and a negative bay in ΔB_z .

The signature at BJA is similar to that at the five high-latitude stations of the Canopus chain. The minimum of the negative bay is accompanied by a maximum in ΔB_y , which is usually associated with the presence of field aligned currents.

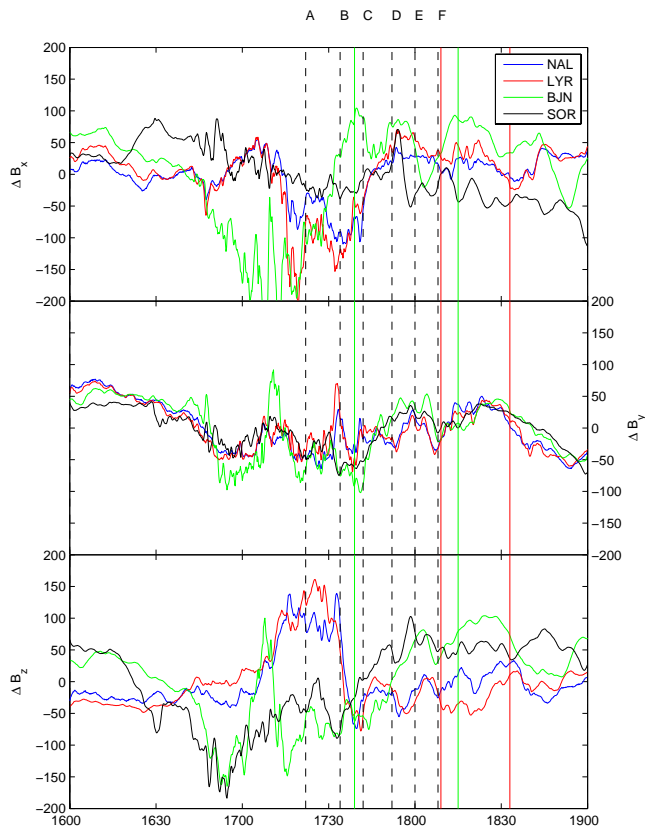


Fig. 9. The ΔB_X , ΔB_Y and ΔB_Z components of the IMAGE chain. For each trace the mean value over the 3 h period is subtracted. The vertical dashed lines represent the times A through F at which SuperDARN measurements are shown in Fig. 10 and the solid vertical lines show the start and end times of the poleward motion of the aurora as in Fig. 6.

The higher 2 stations (LYR and NAL) show a positive bay in ΔB_Z , whereas the lower two stations (SOR and BJJ) show a negative bay with a positive excursion in the middle for BJJ. This indicates that the start of the electrojet and the field aligned currents is somewhere between SOR and BJJ and then successively there is a north-westward motion of the westward electrojet and associated field aligned currents and that the electrojet remains between the lower and higher latitude stations. There is no clear indication in the solar wind or magnetosheath data what sets up this activity, e.g. Cluster shows a rather constant magnetic field in the magnetosheath. The THEMIS spacecraft are in the afternoon sector of the magnetosheath and show little variation in total field strength (at ~ 30 nT). However, before 17:30 UT it can be seen in Fig. 2 that there is the northward turning of the IMF seen by Cluster, TC1 and Geotail. This means that the stopping of the reconnection at the nose of the magnetopause lets the field aligned current region move northward in the IMAGE region. The current systems were already in place at that time, as Fig. 9 clearly shows and the northward turning IMF may only move the current system.

SuperDARN measurements for six times are shown in Fig. 10, which we now can compare, panel-by-panel, with the interpretation of the ground magnetometer data in Fig. 8 where the vertical dashed lines show the times for which the SuperDARN data are shown in Fig. 10 and the vertical solid lines show the start and end times of the auroral poleward motion. The specific times shown in Fig. 10 have been chosen based on maxima in the observed convection during the interval of interest.

In order to visualise the SuperDARN data, we employ the “map potential” technique developed by Ruohoniemi and Baker (1998). This technique yields large-scale global convection maps from the line-of-sight (l-o-s) velocity measurements from multiple radars, via mathematical fitting of the data to an expansion of the electrostatic potential in spherical harmonics. The electric potentials of the solution represent the plasma streamlines of the modelled convection pattern. As backscatter targets are not always available, information from the statistical model of Ruohoniemi and Greenwald (1996), parameterised by IMF conditions, is used to stabilise the solution where no measurements are made. Figure 10 presents Northern Hemisphere ionospheric convection patterns, each averaged over 2-min intervals. Dotted concentric semi-circles indicate lines of constant magnetic latitude in 10 degree increments whilst local noon is located at the top of each plot, midnight at the bottom, dawn on the right-hand side and dusk on the left, as if the observer were looking down from a location above the northern magnetic pole.

The solid (dashed) black lines represent the negative (positive) equipotential contours, and therefore, the ionospheric plasma flow streamlines, determined from the map potential algorithm. The coloured dots indicate locations where radar l-o-s velocity data are available. The vectors drawn from these dots are calculated by combining the measured l-o-s velocity and the component of the convection flow (from the fitted solution) that is orthogonal to the l-o-s direction (i.e. the radar beam) at each location. Both the vectors and the dots are colour coded according to the vector’s velocity magnitude, as indicated by the colour scale; the length of the vector also indicates the magnitude of the velocity at that location.

- A: At $\sim 17:24$ UT the increase in B_H starts for both high and low latitude stations (except for RANK) indicating an increase in the ionospheric currents. SuperDARN data indicate that there is strong ionospheric convection in the post-noon region and near the Geotail footpoint at the same time.
- B: When the B_H levels out at $\sim 17:30$ UT, indicative that the increase of the ionospheric currents has stopped, the ionospheric convection is significantly reduced.
- C: At $\sim 17:42$ UT, the post-noon convection has increased again and moved partly to pre-noon, around which an increase in B_H for the high-latitude stations starts.

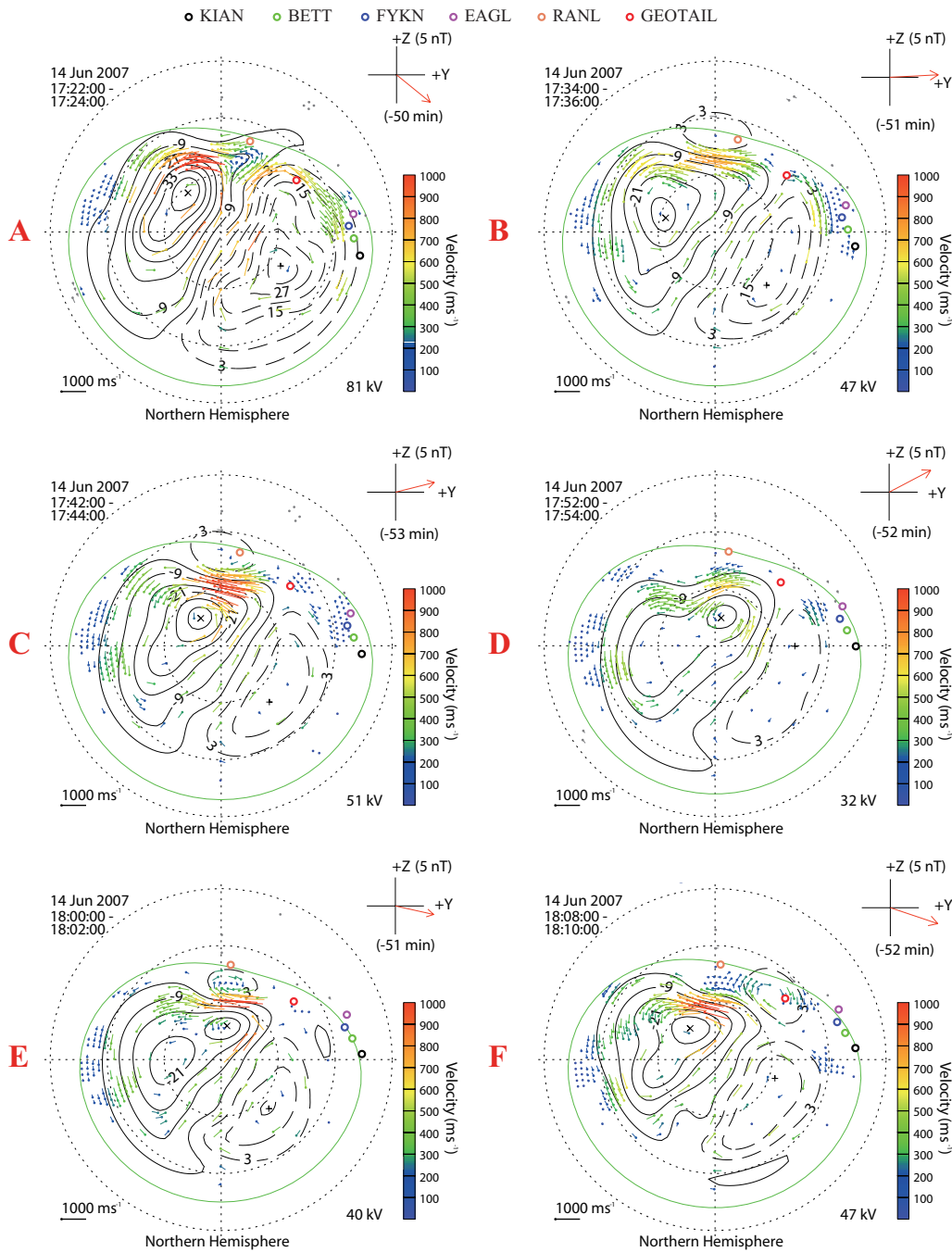


Fig. 10. SuperDARN backscatter and (mainly dayside) convection plots. (A) 17:22–17:24 UT; (B) 17:34–17:36 UT; (C) 17:42–17:44 UT, (D) 17:52–17:54 UT; (E) 18:00–18:02 UT and (F) 18:08–18:10 UT. The coloured circles show the location of the high-latitude ground stations and the traced footprint of Geotail.

D: B_H levels off after a dip for the high latitude stations at $\sim 17:52$, at which time the ionospheric convection starts to reduce, leading to a leveling off of the B_H and subsequent decrease.

E: At $\sim 18:00$ UT the ionospheric convection starts to increase again, with still decreasing B_H

F: At $\sim 18:08$ UT the ionospheric convection has intensified again and both high and low latitude stations show increasing B_H .

It seems that the dayside convection behaviour is well correlated with the magnetic signatures on the ground and their associated currents in the ionosphere. The field aligned

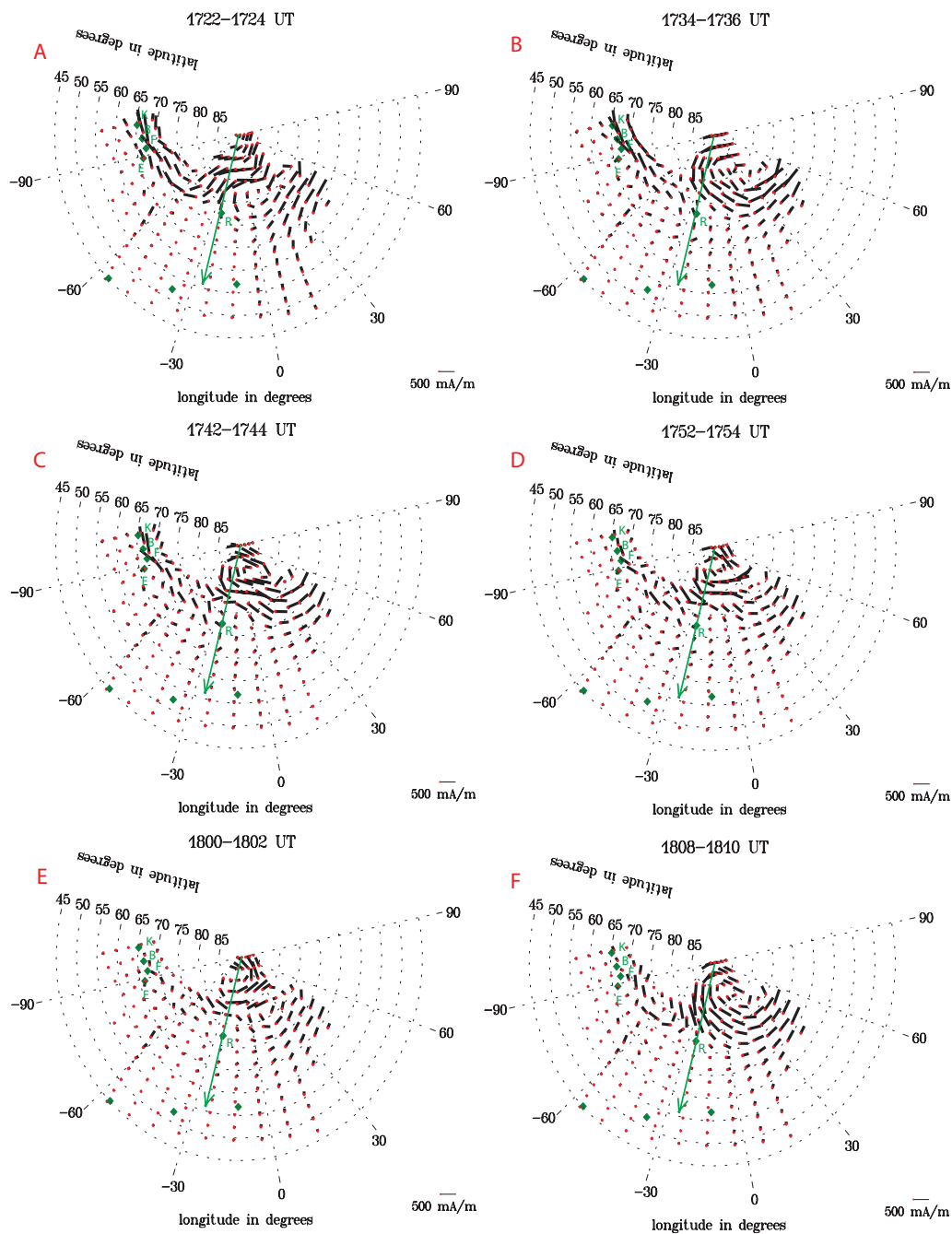


Fig. 11. The averaged equivalent currents for six 2-min intervals. (A) 17:22–17:24 UT; (B) 17:34–17:36 UT; (C) 17:42–17:44 UT, (D) 17:52–17:54 UT; (E) 18:00–18:02 UT and (F) 18:08–18:10 UT. The green dots show the locations of the high/low latitude ground stations from Fig. 8, and RANK is labeled with a green “R”. The direction of the Sun is indicated by the large green arrow in each panel.

currents are associated with the ionospheric drifts through (Chisham et al., 2007):

$$J_{\parallel} = \Sigma_P \mathbf{B} (\nabla \times \mathbf{v}) + (\mathbf{v} \times \mathbf{B}) \cdot \nabla \Sigma_P + |\mathbf{B}| \mathbf{v} \cdot \nabla \Sigma_H, \quad (2)$$

where Σ_P and Σ_H are the Pedersen and Hall conductivity, respectively, and assuming a uniform ionospheric conductance this reduces to:

$$\frac{J_{\parallel}}{\Sigma_P} = \mathbf{B} \cdot (\nabla \times \mathbf{v}). \quad (3)$$

Thus stronger vorticity in the ionosphere drives stronger field aligned currents, which is exactly what is seen in the list above (points A through F) with sometimes a time difference between the convection and the magnetic signature measured on the ground (point E).

In order to compare the SuperDARN and ground signatures better, the latter are turned into equivalent ionospheric currents. In Fig. 11 the averaged equivalent currents (Amm and Viljanen, 1999; Weygand et al., 2011) for the 2 min intervals chosen from the SuperDARN data are shown, based on 48 ground magnetometer stations of the CANMOS, CARISMA, GIMA, Greenland, MACCS and THEMIS GMAG chains. These plots show that RANK is situated in an active region where the currents strongly change direction, when compared with the more westward stations at the same latitude.

Comparing the direction of the ionospheric currents near RANK with the observed flows shows that in the vortex in the currents and the flows are anti-parallel. This is expected when the assumption is made that all the measured currents are Hall currents (see e.g. Untiedt and Baumjohann, 1993; Benkevitch et al., 2006) and if there is no conductance gradient perpendicular to the electric field direction (Amm, 2002). When looking at the SuperDARN and equivalent current maps, overall there is a very good correspondence of the patterns. Also for instance the weakening of the potential at 17:52 UT is clearly seen as a weakening of the currents. Further, the postnoon enhanced flow corresponds to enhanced currents for most of the event. The prenoon flow channel extension at 17:22 UT is well seen in the currents, too. On the other hand, the curl structure at high latitudes e.g. at 17:42 and 17:52 UT is much more pronounced in the equivalent currents than in the SuperDARN data, which is likely due to lack of radar backscatter further north.

3 Discussion

We have followed magnetic field rotations in the solar wind, that interacted with the Earth's bow shock and magnetic field after a long period (≥ 1.5 h) of southward B_z and high solar wind dynamic pressure, with a set of six different spacecraft located all around the Earth. This unique configuration gives us the possibility to observe how solar wind structures interact with and move through the bow shock, magnetosheath and magnetopause.

Before these rotations arrived at the Earth's magnetosphere there was a ~ 1.5 h interval of southward B_z (see Fig. 1) from $\sim 14:45$ till $\sim 16:20$ UT. During this interval the magnetosphere is rather quiet, with a low AE index of ~ 200 nT over a longer period from $\sim 12:00$ till $\sim 16:00$ UT.

The time delay between ACE and Wind does not change between rotations # 1 through 5 even though the orientations of the normals vary strongly and the front is changing from plane to concave and convex. This probably means that all the rotations that are observed are part of one larger structure moving from the Sun towards the Earth. Possibly, observations by STEREO can be used to check if such a large scale structure is moving from the Sun towards the Earth.

We found that the south-north and north-south rotations of the IMF were accompanied by small v_y and v_z variations,

turning the solar wind flow almost completely along the sunward direction when the IMF B_z was northward. There is no significant density variation associated with the first rotation, but for the second there is an increase in density and an almost doubling of the dynamic pressure (see Fig. 1). This means that the expansion of the magnetopause will be less for this interval ($\sim 17:00$ – $17:30$ UT) than would happen during constant solar wind dynamic pressure. The two solar wind monitors (ACE and Wind) show that the normals of the rotation are pointed in different directions. Also, there is a difference in the overall shape of the magnetic signature, which turned out to be a spatial effect when compared with the various spacecraft near Earth, showing a clear pre-noon – post-noon dichotomy.

As expected, the solar wind magnetic field drapes around the Earth's magnetopause. In the solar wind the minimum variance direction of the rotations are mainly aligned with the solar wind direction (see Table 1), however in the magnetosheath we can see that, except for Cluster, the minimum variance directions of the rotations are basically perpendicular to the plasma velocity and the velocity of the magnetic structures resulting from the timing analysis (see Table 3), but still moving with the plasma down the magnetosheath towards the tail. The difference in the Cluster data is the location of the spacecraft in the pre-dawn sector, combined with the direction of the Parker spiral during this period. This tends to bend the magnetic field back again perpendicular to the direction of the magnetosheath along the magnetotail.

The various structures crossing over the spacecraft have different timing order as shown in Table 2. Inside the magnetosheath the propagation of these structures over the various spacecraft is different from that in the solar wind. The normal directions shown in Fig. 3 already indicated that spatial differences occur between Wind and ACE, and the comparison in shape of the magnetic signature with pre- and post-noon spacecraft. The shape of the rotation fronts # 5 and 6 as inferred from the normals at ACE and Wind is concave, similar to rotation # 3. However, the difference in normal direction for # 5 and 6 is much less than for # 3, indicating a less curved front.

Interestingly, none magnetosheath spacecraft show the ~ 12 min length difference associated with the second and shorter sawtooth-looking structure measured by Wind, clearly visible in the B_z traces in Fig. 1. All spacecraft in the magnetosheath observe the second sawtooth-looking structure with the same time length as ACE. This indicates that, apart from the different structures of B_z for the pre- and post-noon spacecraft, there is more spatial structure in the solar wind which we cannot observe due to lack of more solar wind monitors.

Looking at the solar wind data, another difference between the “square” and “sawtooth-looking” structures is that the v_z is positive for the former and negative for the latter. Since TC1 was the northernmost spacecraft in the magnetosheath

(see Fig. 4) this southward motion of the structure may lead to TC1 observing it later than all other spacecraft.

There is a strong deviation of the plasma velocity and the velocity obtained from the timing analysis for THEMIS. The reason for this can be found in the so called Q-parameter (Robert et al., 1998), which determines how well (four of) the spacecraft form a tetrahedron. Clearly from Fig. 5 one can see that the THEMIS spacecraft are mainly lined up along X with a spread in Z (a string-of-pearls configuration), which will limit the accuracy of the direction information that we can obtain from the timing method. Indeed, the timing analysis is dominated by the large elongation in X .

After the long period of southward B_z the magnetosphere has been eroded, which is evident from TC1 and Geotail being in the magnetosheath at radial distances less than $10 R_E$ from the Earth. Combined with the strong dynamic pressure of the solar wind compressing the magnetosphere, this means that any significant change in the solar wind, e.g. a south- to northward turning, will have a strong effect on the location of the magnetopause.

Dušík et al. (2010) recently showed statistically that the cone angle of the solar wind influences the location of the magnetopause, where the difference could be as much as $1 R_E$ for IMF aligned with and IMF perpendicular to the solar wind flow because of a less effective transformation of the solar wind dynamic pressure to the pressure imposed onto the magnetopause during intervals of a radial IMF. Indeed, that is what is observed in Fig. 6: after TC1 measures a south- to northward turning of the magnetic field in the magnetosheath, Geotail gets engulfed by the magnetosphere.

It is clear from Fig. 6 that it takes some time between the polarity change of the magnetic field and the magnetopause reaction. With both spacecraft (TC1 and Geotail) in the magnetosheath just after 17:00 UT, we can see that the SN turning at both spacecraft is separated by ~ 6 min. Looking at the Geotail data, it takes ~ 9 min for the magnetopause to cross over the spacecraft after the SN turning has passed over Geotail.

It was estimated from the keograms that the magnetic field lines move outwards at $\sim 44 \text{ km s}^{-1}$ at the magnetic equator. Note that this is similar to the bow shock velocity that was determined at $\sim 38.5 \text{ km s}^{-1}$. The SN turning at $\sim 17:18$ UT at TC1 takes ~ 6 min to move to Geotail as can be seen in Fig. 6 ($\Delta X_{\text{TC1-Geo}} \approx 4 R_E$). It then takes ~ 12 min for the aurora to start moving poleward and another ~ 9 min for the magnetopause to move over Geotail. The field line outward motion thus takes 9 min to reach Geotail, which means that the field line at the magnetic equator would move $\sim 3 R_E$ outward. Phan et al. (1996) showed that the magnetopause at similar solar wind dynamic pressure was located at $\sim 8.2 R_E$ for small negative $B_z \geq -10 \text{ nT}$ in the magnetosheath. For this event $B_z \sim -20 \text{ nT}$ and thus we can expect the magnetopause to be even closer to Earth. Geotail at (4.73, -9.39 , -1.20) R_E would be well within the nominal magnetopause (see Fig. 3) with its subsolar point at $\sim 11 R_E$ (Fairfield,

1971). Phan et al. (1996) showed that the subsolar point was moved to $8.2 R_E$ under similar circumstances, which would agree well with the estimate $\sim 3 R_E$ outward motion of the magnetopause found in this study.

Looking at the second arrow in Fig. 6 panel (c), we find that after the southward turning measured by TC1 it takes approximately the same time for the auroral poleward motion to stop and return to low latitudes again. However, Geotail moves out of the magnetosphere much earlier, approximately 11 min after TC1 measures the southward turning. The erosion of the magnetopause for southward B_z thus takes longer than the expansion for northward B_z . This might be the reason why after the next northward turning Geotail gets engulfed more quickly than at the first northward turning and the quicker response, i.e. poleward motion, of the aurora.

Although there are only south pole aurora observations, we can compare its activity with the data from ground magnetometers. The start of the poleward motion of the aurora at $\sim 17:45$ UT happens during the increase in B_H . This is in agreement with the poleward motion of the aurora. The motion is related to increased ionospheric convection (see Fig. 10 panel c). The poleward motion of the aurora at $\sim 18:20$ UT is only related to an increase in the B_H component. It should also be noted that the B_D component of RANK is similar to that of the low latitude stations, which is in agreement with the discussion above that in the beginning RANK is on the low-latitude side of the field aligned current.

The data from the ground magnetometer chains, transformed to equivalent ionospheric currents, were compared with the SuperDARN radar data. It was shown that there was good correspondence between both data sets: enhanced flows corresponding to increased currents. Slight discrepancies between the two data sets are most likely due to a lack of radar back-scattering, as clearly the region of interest is on the border of the viewing of the SuperDARN radars.

How do the results from this study compare to other observations? The draping of the IMF over the Earth's magnetosphere was studied by Coleman (2005) using Geotail and Interball-Tail data. This was done in order to study whether "perfect draping" (i.e. the clock angle of the magnetic field $\theta_c = \text{atan}\{B_z/B_y\}$ does not change through the draping) takes place. In the study it was found that 30% of the events showed perfect draping (i.e. $\Delta\theta_c \pm 10^\circ$) and 70% of the events were within $\pm 30^\circ$. The draping in this current paper shows that the variation in clock angle is $0 \leq \theta_c \leq 40^\circ$, as shown in Fig. 2 bottom panel. The larger differences between Wind and the other spacecraft observed after $\sim 19:00$ UT are caused by incorrect time shifts of the data for those structures. Our data set fits well in the 70% as found by Coleman (2005).

Recently Wiltberger et al. (2003) studied magnetopause erosion using an MHD code, where they showed a marked delay between the arrival of the southward B_z and the motion of the magnetopause, where a delay of up to 20 min is expected from the build-up of nightside current systems which

drives the decrease of the dayside field. However, the motion of the open-closed field line boundary at the poles is almost simultaneous (on the scale of minutes) with the arrival of the southward B_z at the magnetopause. The study of this current paper shows indeed that the arrival of the southward B_z has a direct influence on the location of the open-closed field line boundary (as shown from the keograms), however, the inward motion of the magnetopause is also almost simultaneous. This can be explained by the fact that the nightside current systems have already been set in place by the previous interval of southward IMF.

Observations by Pitout et al. (2006) with Cluster near the mid-altitude cusp showed that for northward turnings of the IMF there was a quick poleward displacement of the cusp. During multiple directional changes of the IMF the cusp crossed over Cluster back and forth repeatedly. The cusp reacts very fast to these changes in IMF, and they conclude that the reconnection quickly reorganizes, within a few minutes, not unlike what Wiltberger et al. (2003) found. Measurements showed that the cusp poleward boundary moved at (at least) $\sim 30 \text{ km s}^{-1}$ in the north-south direction. This velocity is comparable with the estimated field line velocity found from the keograms in this paper. Similarly, Geotail was crossed by the magnetopause repeatedly, linked to IMF turnings. The magnetosphere has been prepared by the long southward B_z interval before the rotational structures, so that it can react immediately to changes in the IMF, unlike the numerical model of Wiltberger et al. (2003).

4 Summary and conclusions

In this paper we have used a unique set of combined space and ground based monitors to investigate the response of the Earth's magnetosphere to rotations of the IMF B_z from southward to northward and vice-versa. For the first time there are multi-spacecraft missions at both the dawn flank (Cluster) and the dusk flank (THEMIS) whilst two other missions (Geotail and TC1) are located near the subsolar point of the magnetopause. These space data are enhanced with a set of various ground based observations by magnetometers (CARISMA, IMAGE), radar (SuperDARN) and a south-polar auroral camera.

A quick summary of the event is given below:

- Long southward IMF and high ram pressure before rotations have eroded the magnetopause;
- Fast south-north and north-south rotations of the IMF are observed by Wind and ACE;
- Rotational fronts are not always plane between Wind and ACE, but can be curved concave and convex;
- There is spatial difference between the two sawtooth-looking rotations, which also shows up as a difference in pre- and post-noon spacecraft in the magnetosheath;

- The rotations pass the bow shock and the field strength increases accordingly (in agreement with the quasi-perpendicular shock relations for THEMIS A) and the IMF drapes around the magnetopause;
- Timing analysis and plasma data show that the rotations are moving with the plasma (frozen in);
- Northward turning of the IMF:
 - an immediate expansion of the magnetosphere (Geotail);
 - poleward moving aurora (south pole observatory);
 - strong ionospheric currents (ground magnetometers and equivalent currents);
 - strong convection (superDARN radar);
 - northwest-ward moving electrojet and field aligned currents (IMAGE)
- Southward turning of the IMF:
 - erodes the magnetosphere quickly;
 - equatorward motion of the aurora;
 - decrease of the ionospheric convection;
 - weakening of the ionospheric currents;

Comparing pre- and post-noon spacecraft, it has been shown that the rotations of the IMF have a spatial variation over the pre-post noon direction. In the magnetosheath the magnetic field is draped around the magnetopause and the rotations are moving with the plasma flow (frozen in) down the tail, although the normals of the rotations are perpendicular to the flow through the draping effect.

Through a long period of southward IMF B_z and high solar wind dynamic pressure the magnetopause has been eroded significantly. After northward turning of the field the magnetopause moves outward, resulting in poleward moving aurora and the engulfing of Geotail by the magnetosphere. The following southward turning erodes the magnetopause again, letting Geotail enter the magnetosheath again and stopping the poleward motion of the aurora. The erosion of the magnetosphere after the next southward turning of the IMF is slower than the expansion after the northward turning, indicated by the fact that Geotail is engulfed much earlier by the magnetosphere after the following northward turning.

The associated magnetospheric and ionospheric currents show their signatures in the ground magnetometers and the associated ionospheric convection following/driving the current were measured by SuperDARN.

The reaction of the magnetopause and the ionospheric and field aligned currents to changes in the magnetosheath B_z is almost immediate, allowing for the advection time from the spacecraft closest to the magnetopause.

This has been a very clear and clean example of the interaction of a high ram-pressure solar wind IMF rotations

with the Earth's magnetosphere after an extended period of southward IMF B_z for which an almost perfect conjunction of spacecraft in the magnetosheath was available.

Acknowledgements. Part of the work was done for the ISSI working group "Conjugate response of the dayside magnetopause and dawn/dusk flanks using Cluster-THEMIS conjunctions and ground based observations." This work is partly supported by Chinese Academy of Sciences (CAS) visiting Professorship for senior international scientists grant no. 2009S1-54 and the Specialized Research Fund for State Key Laboratories of the CAS. The authors acknowledge the DART system at ISAS for the Geotail data and the Cluster Active Archive (CAA). The all-sky cameras in Antarctica are supported through NSF grants ANT-0636899 and ANT-0636978. JPE holds an STFC advanced fellowship at ICL. We thank the institutes who maintain the IMAGE Magnetometer Array.

Topical Editor I. A. Daglis thanks two anonymous referees for their help in evaluating this paper.

References

- Amm, O.: The method of characteristics for calculating ionospheric electrodynamic from multi-satellite and ground-based radiar data, *J. Geophys. Res.*, 107, 1270, doi:10.1029/2001JA005077, 2002.
- Amm, O. and Viljanen, A.: Ionospheric disturbance magnetic field continuation from the ground to the ionosphere using spherical elementary current systems, *Earth, Planets and Space*, 51, 431–440, 1999.
- Auster, H. U., Glassmeier, K. H., Magnes, W., Aydogar, O., Baumjohann, W., Constantinescu, D., Fischer, D., Fornacon, K. H., Georgescu, E., Harvey, P., Hillenmaier, O., Kroth, R., Ludlam, M., Narita, Y., Nakamura, R., Okrafka, K., Plaschke, F., Richter, I., Schwarzl, H., Stoll, B., Valavanoglou, A., and Wiedemann, M.: The THEMIS fluxgate magnetometer, *Space Sci. Rev.*, 141, 235–264, doi:10.1007/s11214-008-9365-9, 2008.
- Balogh, A., Carr, C. M., Acuña, M. H., Dunlop, M. W., Beek, T. J., Brown, P., Fornacon, K.-H., Georgescu, E., Glassmeier, K.-H., Harris, J., Musmann, G., Oddy, T., and Schwingenschuh, K.: The Cluster Magnetic Field Investigation: overview of in-flight performance and initial results, *Ann. Geophys.*, 19, 1207–1217, doi:10.5194/angeo-19-1207-2001, 2001.
- Benkevitch, L. V., Koustov, A. V., Liang, J., and Watermann, J. F.: Comparison of the magnetic equivalent convection direction and ionospheric convection observed by the SuperDARN radars, *Ann. Geophys.*, 24, 2981–2990, doi:10.5194/angeo-24-2981-2006, 2006.
- Berchem, J. and Russell, C. T.: The thickness of the magnetopause current layer: ISEE 1 and 2 observations, *J. Geophys. Res.*, 87, 2108–2114, 1982.
- Burgess, D.: Collisionless shocks, in: *Introduction to Space Physics*, edited by: Kivelson, M. G. and Russell, C. T., pp. 129–163, Cambridge University Press, Cambridge, 1995.
- Cai, H. T., McCreia, I. W., Dunlop, M. W., Davies, J. A., Bogdanova, Y. V., Pitout, F., Milan, S. E., Lockwood, M., and Ma, S. Y.: Cusp observations during a sequence of fast IMF B_z reversals, *Ann. Geophys.*, 27, 2721–2737, doi:10.5194/angeo-27-2721-2009, 2009.
- Carr, C., Brown, P., Zhang, T. L., Gloag, J., Horbury, T., Lucek, E., Magnes, W., O'Brien, H., Oddy, T., Auster, U., Austin, P., Aydogar, O., Balogh, A., Baumjohann, W., Beek, T., Eichelberger, H., Fornacon, K.-H., Georgescu, E., Glassmeier, K.-H., Ludlam, M., Nakamura, R., and Richter, I.: The Double Star magnetic field investigation: instrument design, performance and highlights of the first year's observations, *Ann. Geophys.*, 23, 2713–2732, doi:10.5194/angeo-23-2713-2005, 2005.
- Chisham, G., Lester, M., Milan, S. E., Freeman, M. P., Bristow, W. A., Grocott, A., McWilliams, K. A., Ruohoniemi, J. M., Yeoman, T. K., Dyson, P. L., Greenwald, R. A., Kikuchi, T., Pinnock, M., Rash, J. P. S., Sato, N., Sofko, G. J., Villain, J.-P., and Walker, A. D. M.: A decade of the Super Dual Auroral Radar Network (SuperDARN): scientific achievements, new techniques and future directions, *Surv. Geophys.*, 28, 33–109, doi:10.1007/s10712-007-9017-8, 2007.
- Coleman, I. J.: A multi-spacecraft survey of magnetic field line draping in the dayside magnetosheath, *Ann. Geophys.*, 23, 885–900, doi:10.5194/angeo-23-885-2005, 2005.
- Dušík, Š., Granko, G., Šafránková, J., Němeček, Z., and Jelínek, K.: IMF cone angle control of the magnetopause location: Statistical study, *Geophys. Res. Lett.*, 37, L19103, doi:10.1029/2010GL044965, 2010.
- Fairfield, D. H.: Avarage and unusual locations of the Earth's magnetopause and bow shock, *J. Geophys. Res.*, 76, 6700–6716, 1971.
- Farrugia, C. J., Burlaga, L. F., Osherovich, V. A., Richardson, I. G., Freeman, M. P., Lepping, R. P., and Lazarus, A. J.: A study of an expanding interplanetary magnetic cloud and its interaction with the Earth's magnetosphere: The interplanetary aspect, *J. Geophys. Res.*, 98, 7621–7632, 1993a.
- Farrugia, C. J., Richardson, I. G., Burlaga, L. F., Osherovich, V. A., and Lepping, R. P.: Simultaneous observations of Solar MeV particles in a magnetic cloud and in the Earth's northern tail lobe: Implications for the global field line topology of magnetic clouds and entry of solar particles into taillobe during cloud passage, *J. Geophys. Res.*, 98, 15497–15507, 1993b.
- Farrugia, C. J., Erkaev, N. V., Biernat, H. K., and Burlaga, L. F.: Anomalous magnetosheath properties during Earth passage of an interplanetary magnetic cloud, *J. Geophys. Res.*, 100, 19245–19258, 1995.
- Farrugia, C. J., Popecki, M., Möbius, E., Jordanova, V. K., Desai, M. I., Fitzenreiter, R. J., Matsui, K. W. O. H., Lepri, S., Zurbuchen, T., Mason, G. M., Lawrence, G. R., Burlaga, L. F., Lepping, R. P., Dwyer, J., and McComas, D.: Wind and ACE observations during the great flow of 1–4 May 1998: Relation to solar activity and implications for the magnetosphere, *J. Geophys. Res.*, 107, 1240, doi:10.1029/2001JA000188, 2002.
- Fear, R. C., Milan, S. E., Fazakerley, A. N., Lucek, E. A., Cowley, S. W. H., and Dandouras, I.: The azimuthal extent of three flux transfer events, *Ann. Geophys.*, 26, 2353–2369, doi:10.5194/angeo-26-2353-2008, 2008.
- Harvey, C. C.: Spatial gradients and volumetric tensor, in: *Analysis Methods for Multi-Spacecraft Data*, edited by: Paschmann, G. and Daly, P., pp. 307–322, ESA, Noordwijk, 1998.
- Hasegawa, H., Wang, J., Dunlop, M. W., Pu, Z. Y., Zhang, Q.-H., Lavraud, B., Taylor, M. G. G. T., Constantinescu, O. D., Berchem, J., Angelopoulos, V., McFadden, J. P., Frey, H. U., Panov, E. V., Volwerk, M., and Bogdanova, Y. V.: Evidence

- for a flux transfer event generated by multiple X-line reconnection at the magnetopause, *Geophys. Res. Lett.*, 37, L16101, doi:10.1029/2010GL044219, 2010.
- Hu, R., Bogdanova, Y. V., Owen, C. J., Foullon, C., Fazakerley, A. N., and Rème, H.: Cluster observations of the midaltitude cusp under strong northward interplanetary magnetic field, *J. Geophys. Res.*, 113, A07S05, doi:10.1029/2007JA012726, 2007.
- Ivchenko, N. V., Sibeck, D. G., Takahashi, K., and Kokubun, S.: A statistical study of the magnetosphere boundary crossings by the Geotail satellite, *G. Geophys. Res.*, 27, 2881–2884, doi:10.1029/2000GL000020, 2000.
- Keika, K., Nakamura, R., Baumjohann, W., Runov, A., Takada, T., Volwerk, M., Zhang, T. L., Klecker, B., Lucek, E. A., Carr, C., Rème, H., Dandouras, I., André, M., and Frey, H.: Response of the inner magnetosphere and the plasma sheet to a sudden impulse, *J. Geophys. Res.*, 113, A07S35, doi:10.1029/2007JA012763, 2008.
- Keika, K., Nakamura, R., Baumjohann, W., Angelopoulos, V., Kabin, K., Glassmeier, K. H., Sibeck, D. G., Magnes, W., Auster, H. U., Fornaçon, K. H., McFadden, J. P., Carlson, C. W., Lucek, E. A., Carr, C. M., Dandouras, I., and Rankin, R.: Deformation and evolution of solar wind discontinuities through their interactions with the Earth's bow shock, *J. Geophys. Res.*, 114, A00C26, doi:10.1029/2008JA013481, 2009.
- Kokubun, S., Yamamoto, T., Acuña, M. H., Hayashi, K., and Kawano, K. S.: The GEOTAIL magnetic field experiment, *J. Geomagn. Geoelectr.*, 46, 7–21, 1994.
- Korotova, G. I., Sibeck, D. G., and Rosenberg, T.: Geotail observations of FTE velocities, *Ann. Geophys.*, 27, 83–92, doi:10.5194/angeo-27-83-2009, 2009.
- Laundal, K. M., Østgaard, N., Snekvik, K., and Frey, H. U.: Interhemispheric observations of emerging polar cap asymmetries, *J. Geophys. Res.*, 115, A07230, doi:10.1029/2009JA015160, 2010.
- Lavraud, B. and Borovsky, J. E.: Altered solar wind-magnetosphere interaction at low Mach numbers: Coronal mass ejections, *J. Geophys. Res.*, 113, A00B08, doi:10.1029/2008JA013192, 2008.
- Lavraud, B., Fedorov, A., Budnik, E., Grigoriev, A., Cargill, P. J., Dunlop, M. W., Rème, H., Dandouras, I., and Balogh, A.: Cluster survey of the high-altitude cusp properties: a three-year statistical study, *Ann. Geophys.*, 22, 3009–3019, doi:10.5194/angeo-22-3009-2004, 2004.
- Lavraud, B., Fedorov, A., Budnik, E., Thomsen, M. F., Grigoriev, A., Cargill, P. J., Dunlop, M. W., Rème, H., Dandouras, I., and Balogh, A.: High-altitude cusp flows dependence on IMF orientation: A three-year Cluster statistical study, *J. Geophys. Res.*, 110, A02209, doi:10.1029/2004JA010804, 2005.
- Lepping, R. P., Acuña, M. H., Burlaga, L. F., Farrell, W. M., Slavin, J. A., Schatten, K. H., Mariani, F., Ness, N. F., Neubauer, F. M., Whang, Y. C., Byrnes, J. B., Kennon, R. S., Panetta, P. V., Scheifele, J., and Worley, E. M.: The Wind Magnetic Field Investigation, *Space Sci. Rev.*, 71, 207–229, 1995.
- Lin, R. P., Anderson, K. A., Ashford, S., Carlson, C., Curtis, D., Ergun, R., McFadden, D. L. J., McCarthy, M., Parks, G. K., Rème, H., Bosqued, J. M., Coutelier, J., Cotin, F., D'Uston, C., Wenzel, K.-P., Sanderson, T. R., Henrion, J., Ronnet, J. C., and Paschmann, G.: A Three-Dimensional Plasma and Energetic Particle Investigation for the Wind Spacecraft, *Space Sci. Rev.*, 71, 125–153, 1995.
- Lockwood, M., Fazakerley, A., Opgenoorth, H., Moen, J., van Eyken, A. P., Dunlop, M., Bosqued, J.-M., Lu, G., Cully, C., Eglitis, P., McCrea, I. W., Hapgood, M. A., Wild, M. N., Stamper, R., Denig, W., Taylor, M., Wild, J. A., Provan, G., Amm, O., Kauristie, K., Pulkkinen, T., Strømme, A., Prikrýl, P., Pitout, F., Balogh, A., Rème, H., Behlke, R., Hansen, T., Greenwald, R., Frey, H., Morley, S. K., Alcaydè, D., Brelly, P.-L., Donovan, E., Engebretson, M., Lester, M., Watermann, J., and Maruccci, M. F.: Coordinated Cluster and ground-based instrument observations of transient changes in the magnetopause boundary layer during an interval of predominantly northward IMF: relation to reconnection pulses and FTE signatures, *Ann. Geophys.*, 19, 1613–1640, doi:10.5194/angeo-19-1613-2001, 2001.
- Lockwood, M., Moen, J., van Eyken, A. P., Davies, J. A., Okavik, K., and McCrea, I. W.: Motion of the dayside polar cap boundary during substorm cycles: I. Observations of pulses in the magnetopause reconnection rate, *Ann. Geophys.*, 23, 3495–3511, doi:10.5194/angeo-23-3495-2005, 2005.
- Lui, A. T. Y., Sibeck, D. G., Phan, T., Angelopoulos, V., McPhadden, J., Carlson, C., Larson, D., Bonnell, J., Glassmeier, K.-H., and Frey, S.: Reconstruction of a magnetic flux rope from THEMIS observations, *Geophys. Res. Lett.*, 35, L17S05, doi:10.1029/2007GL032933, 2008.
- Lundin, R.: On the magnetospheric boundary layer and solar wind energy transfer into the magnetosphere, *Space Sci. Rev.*, 48, 263–320, 1988.
- McComas, D. J., Bame, S. J., Barker, P., Feldman, W. C., Phillips, J. L., Riley, P., and Griffée, J.: Solar Wind Electron Proton Alpha Monitor (SWEPAM) for the Advanced Composition Explorer, *Space Sci. Rev.*, 86, 563–612, 1998.
- McFadden, J. P., Carlson, C. W., Larson, D., Ludlam, M., Abiad, R., Elliott, B., Turin, P., Marckwordt, M., and Angelopoulos, V.: The THEMIS ESA plasma instrument and in-flight calibration, *Space Sci. Rev.*, 141, 277–302, doi:10.1007/s11214-008-9440-2, 2008.
- Mühlbachler, S., Farrugia, C. J., Biernat, H. K., and Torbert, R. B.: The geostationary field during dayside erosion events 1996–2001: A joint Wind, ACE, and GOES study, *J. Geophys. Res.*, 108, 1418, doi:10.1029/2003JA009833, 2003.
- Mühlbachler, S., Semenov, V. S., Biernat, H. K., Erkaev, N. V., Kubyskin, I. V., Farrugia, C. J., Langmayr, D., and Vogl, D. F.: A reconnection model describing erosion of the magnetopause and the associated bow shock motion, *Adv. Space Res.*, 33, 2103–2107, doi:10.1016/j.asr.2003.04.052, 2004.
- Mukai, T., Machida, S., Saito, Y., Hirahara, M., Terasawa, T., Kaya, N., Obara, T., Ejiri, M., and Nishida, A.: The Low Energy Particle (LEP) experiment onboard the GEOTAIL Satellite, *J. Geomagn. Geoelectr.*, 46, 669–692, 1994.
- Nishida, A.: IMF control of the Earth's magnetosphere, *Space Sci. Rev.*, 34, 185–200, 1983.
- Østgaard, N., Mende, S. B., Frey, H. U., Immel, T. J., Frank, L. A., Sigwarth, J. B., and Stubbs, T. J.: Interplanetary magnetic field control of the location of substorm onset and auroral features in the conjugate hemispheres, *J. Geophys. Res.*, 109, A07204, doi:10.1029/2003JA010370, 2004.
- Østgaard, N., Tsyganenko, N., Mende, S. B., Frey, H. U., Immel, T. J., Fillingim, M., Frank, L. A., and Sigwarth, J. B.: Observations and model predictions of substorm auroral asymmetries in the conjugate hemispheres, *Geophys. Res. Lett.*, 32, L05111,

- doi:10.1029/2004GL022166, 2005.
- Pallochia, G., Samsonov, A. A., Bavassano Cattaneo, M. B., Maruccci, M. F., Rème, H., Carr, C. M., and Cao, J. B.: Interplanetary shock transmitted into the Earth's magnetosheath: Cluster and Double Star observations, *Ann. Geophys.*, 28, 1141–1156, doi:10.5194/angeo-28-1141-2010, 2010.
- Parkinson, M. L., Pinnock, M., Wild, J. A., Lester, M., Yeoman, T. K., Milan, S. E., Ye, H., Devlin, J. C., Frey, H. U., and Kikuchi, T.: Interhemispheric asymmetries in the occurrence of magnetically conjugate sub-auroral polarisation streams, *Ann. Geophys.*, 23, 1371–1390, doi:10.5194/angeo-23-1371-2005, 2005.
- Paschmann, G. and Daly, P.: *Analysis Methods for Multi-Spacecraft Data*, ESA, Noordwijk, 1998.
- Paschmann, G. and Daly, P.: *Multi-Spacecraft Analysis Methods Revisited*, ESA, Noordwijk, 2008.
- Phan, T. D., Larson, D. E., Lin, R. P., McFadden, J. P., and C. W. Carlson, K. A. A., Ergun, R. E., Ashford, S. M., McCarthy, M. P., Parks, G. K., Rème, H., Bosqued, J. M., D'Uston, C. D., Wenzel, K. P., Sanderson, T. R., and Szabo, A.: The subsolar magnetosheath and magnetopause for high solar wind ram pressure: WIND observations, *Geophys. Res. Lett.*, 23, 1279–1282, doi:10.1029/96GL00845, 1996.
- Pitout, F., Escoubet, C. P., Georgescu, Y. V. B. E., Fazakerley, A. N., and Rème, H.: Response of the mid-altitude cusp to rapid rotations of the IMF, *Geophys. Res. Lett.*, 33, L11107, doi:10.1029/2005GL025460, 2006.
- Pudovkin, M. I., Zaitseva, S. A., and Besser, B. P.: The magnetopause erosion and the magnetosheath magnetic field penetration into the dayside magnetosphere, *Adv. Space Res.*, 19, 1909–1912, doi:10.1016/S0273-1177(97)00099-9, 1997.
- Rème, H., Aoustin, C., Bosqued, J. M., Dandouras, I., Lavraud, B., Sauvaud, J. A., Barthe, A., Bouyssou, J., Camus, Th., Coeur-Joly, O., Cros, A., Cuvilo, J., Ducay, F., Garbarowitz, Y., Medale, J. L., Penou, E., Perrier, H., Romefort, D., Rouzard, J., Vallat, C., Alcaydé, D., Jacquey, C., Mazelle, C., d'Uston, C., Möbius, E., Kistler, L. M., Crocker, K., Granoff, M., Mouikis, C., Popecki, M., Vosbury, M., Klecker, B., Hovestadt, D., Kucharek, H., Kuenneth, E., Paschmann, G., Scholer, M., Sckopke, N., Seidenschwang, E., Carlson, C. W., Curtis, D. W., Ingraham, C., Lin, R. P., McFadden, J. P., Parks, G. K., Phan, T., Formisano, V., Amata, E., Bavassano-Cattaneo, M. B., Baldetti, P., Bruno, R., Chionchio, G., Di Lellis, A., Maruccci, M. F., Pallochia, G., Korth, A., Daly, P. W., Graeve, B., Rosenbauer, H., Vasylunas, V., McCarthy, M., Wilber, M., Eliasson, L., Lundin, R., Olsen, S., Shelley, E. G., Fuselier, S., Ghielmetti, A. G., Lennartsson, W., Escoubet, C. P., Balsiger, H., Friedel, R., Cao, J.-B., Kovrazhkin, R. A., Papamastorakis, I., Pellat, R., Scudder, J., and Sonnerup, B.: First multispacecraft ion measurements in and near the Earth's magnetosphere with the identical Cluster ion spectrometry (CIS) experiment, *Ann. Geophys.*, 19, 1303–1354, doi:10.5194/angeo-19-1303-2001, 2001.
- Robert, P., Harvey, C. C., Dunlop, M. V., Daly, P. W., and Glassmeier, K.-H.: Tetrahedron Geometric Factors, in: *Analysis Methods for Multi-Spacecraft Data*, edited by: Paschmann, G. and Daly, P., pp. 323–348, ESA, Noordwijk, 1998.
- Ruohoniemi, J. M. and Baker, K. B.: Large-scale imaging of high-latitude convection with Super Dual Auroral Radar Network HF radar observations, *J. Geophys. Res.*, 103, 20797–20811, 1998.
- Ruohoniemi, J. M. and Greenwald, R. A.: Statistical patterns of high-latitude convection obtained from Goose Bay HF radar observations, *J. Geophys. Res.*, 101, 21746–21763, 1996.
- Sandholt, P. E. and Farrugia, C. J.: Monitoring magnetosheath-magnetosphere interconnection topology from the aurora, *Ann. Geophys.*, 20, 629–637, doi:10.5194/angeo-20-629-2002, 2002.
- Sandholt, P. E., Farrugia, C. J., Moen, J., Noraberg, Ø., Lubek, B., Sten, T., and Hansen, T.: A classification of dayside aurora forms and activities as a function of interplanetary magnetic field orientation, *J. Geophys. Res.*, 103, 23325–23345, 1998.
- Sandholt, P. E., Farrugia, C. J., and Denig, W. F.: Dayside aurora and the role of IMF $|B_y|/|B_z|$: detailed morphology and response to magnetopause reconnection, *Ann. Geophys.*, 22, 613–628, doi:10.5194/angeo-22-613-2004, 2004.
- Schwartz, S. J.: Shock and discontinuity normals, Mach numbers, and related parameters, in: *Analysis Methods for Multi-Spacecraft Data*, edited by: Paschmann, G. and Daly, P., pp. 249–270, ESA, Noordwijk, 1998.
- Sckopke, N., Paschmann, G., Bame, S. J., Gosling, J. T., and Russell, C. T.: Evolution of ion distributions across the nearly perpendicular bow shock: specularly and non-specularly reflected-gyrating ions, *J. Geophys. Res.*, 88, 1621–1636, 1983.
- Shue, J.-H., Song, P., Russell, C. T., Thomsen, M. F., and Petrinec, S. M.: Dependence of magnetopause erosion on southward interplanetary magnetic field, *J. Geophys. Res.*, 106, 18777–18788, doi:10.1029/2001JA900039, 2001.
- Sibeck, D. G.: A model for the transient magnetospheric response to sudden solar wind dynamic pressure variations, *J. Geophys. Res.*, 95, 3755–3771, 1990.
- Sibeck, D. G. and Gosling, J. T.: Magnetosheath density fluctuations and magnetopause motion, *J. Geophys. Res.*, 101, 31–40, 1996.
- Sibeck, D. G. and Siscoe, G. L.: Downstream properties of magnetic flux transfer events, *J. Geophys. Res.*, 89, 10709–10715, 1984.
- Sibeck, D. G., Lopez, R. E., and Roelof, E. C.: Solar wind control of the magnetopause shape, location and motion, *J. Geophys. Res.*, 96, 5489–5495, 1991.
- Sibeck, D. G., Kudela, K., Lepping, R. P., Lin, R., Nemecek, Z., Nozdrachev, M. N., Phan, T.-D., Prech, L., Safankova, J., Singer, H., and Yermolaev, Y.: Magnetopause motion driven by interplanetary magnetic field variations, *J. Geophys. Res.*, 105, 25155–25169, 2000.
- Smith, E. J.: Identification of interplanetary tangential and rotational discontinuities, *J. Geophys. Res.*, 78, 2054–2063, 1973.
- Smith, C. W., L'Heureux, J., Ness, N. F., Acuña, M. H., and Scheifele, L. F. B.: The ACE Magnetic Fields Experiment, *Space Sci. Rev.*, 86, 613–632, doi:10.1023/A:1005092216668, 1998.
- Untiedt, J. and Baumjohann, W.: Studies of polar current systems using the IMS Scandinavian magnetometer array, *Space Sci. Rev.*, 63, 245–390, 1993.
- Volwerk, M.: Multi-Satellite observations of ULF waves, in: *Magnetospheric ULF waves: Synthesis and new directions*, edited by: Takahashi, K., Chi, P. J., Denton, R. E., and Lysak, R. L., pp. 109–135, AGU, Washington, 2006.
- Wang, J., Dunlop, M. W., Pu, Z. Y., Zhou, X. Z., Zhang, X. G., Wei, Y., Fu, S. Y., Xiao, C. J., Fazakerley, A., Laakso, H., Taylor, M. G. G. T., Bogdanova, Y., Pitout, F., Davies, J., Zong, Q. G., Shen, C., Liu, Z. X., Carr, C., Perry, C., Rème, H., Dandouras,

- I., Escoubet, P., and Owen, C. J.: TC1 and Cluster observation of an FTE on 4 January 2005: A close conjunction, *Geophys. Res. Lett.*, 37, L03106, doi:10.1029/2006GL028241, 2007.
- Weygand, J. M., Amm, O., Viljanen, A., Angelopoulos, V., Murr, D., Engebretson, M., Gleisner, H., and Mann, I.: Application and validation of the spherical elementary currents systems technique for deriving ionospheric equivalent currents with the North American and Greenland ground magnetometer arrays, *J. Geophys. Res.*, 116, A03305, doi:10.1029/2010JA016177, 2011.
- Wild, J. A., Milan, S. E., Owen, C. J., Bosqued, J. M., Lester, M., Wright, D. M., Frey, H., Carlson, C. W., Fazakerley, A. N., and Rème, H.: The location of the open-closed magnetic field line boundary in the dawn sector auroral ionosphere, *Ann. Geophys.*, 22, 3625–3639, doi:10.5194/angeo-22-3625-2004, 2004.
- Wild, J. A., Milan, S. E., Cowley, S. W. H., Bosqued, J. M., Rème, H., Nagai, T., Kokubun, S., Saito, Y., Mukai, T., Davies, J. A., Cooling, B. M. A., Balogh, A., and Daly, P. W.: Simultaneous in-situ observations of the signatures of dayside reconnection at the high- and low-latitude magnetopause, *Ann. Geophys.*, 23, 445–460, doi:10.5194/angeo-23-445-2005, 2005.
- Wiltberger, M., Lopez, R. E., and Lyon, J. G.: Magnetopause erosion: A global view from MHD simulation, *J. Geophys. Res.*, 108, 1235, doi:10.1029/2002JA009564, 2003.
- Zhang, H., Zong, Q.-G., Sibeck, D. G., Fritz, T. A., McPhadden, J. P., Glassmeier, K.-H., and Larson, D.: Dynamic motion of the bow shock and the magnetopause observed by THEMIS spacecraft, *J. Geophys. Res.*, 114, A00C12, doi:10.1029/2008JA013488, 2009.
- Zhang, T. L., Baumjohann, W., Nakamura, R., Volwerk, M., Runov, A., Vörös, Z., Glassmeier, K.-H., and Balogh, A.: Neutral sheet normal direction determination, *Adv. Space Res.*, 36, 1940–1945, 2005.
- Zwan, B. J. and Wolf, R. A.: Depletion of solar wind plasma near a planetary boundary, *J. Geophys. Res.*, 81, 1636–1648, 1976.